
CRS4
Center for Advanced Studies,
Research and Development in Sardinia
Uta - (CA)

Inviscid Supersonic Minimum Length Nozzle Design

G. Delussu and M. Talice
Computational Fluid Dynamics Area, CRS4, Italy

Date: December 17th 2002

Contents

1	Introduction	3
2	Convergent Section Design	4
2.1	Pressure Gradient Criterion	4
2.2	Geometric Shape Criterion	6
2.3	Conclusions	8
3	Divergent Section Design	11
3.1	Two-dimensional Divergent Section Design	13
3.1.1	Numerical Methods	16
3.2	Axisymmetric Divergent Section Design	18
3.2.1	Numerical Methods	21
3.3	Conclusions	21
4	Results	23
4.1	Inviscid Computations	25
4.2	Viscous Computations	36
5	Conclusions	45

Abstract

An aerospace vehicle is accelerated by a propulsion system to a given velocity. A nozzle is used to extract the maximum thrust from high pressure exhaust gases generated by the propulsion system. The nozzle is responsible for providing the thrust necessary to successfully accomplish the mission while its design efficiency translates to greater payload and reduction in propellant consumption.

Specifically, the nozzle is that portion of the engine beyond the combustion chamber. Typically, the combustion chamber is a constant area duct into which propellants are injected, mixed and burned. Its length is sufficient to complete the combustion of the propellants before the nozzle accelerates the gas products. The nozzle is said to begin at the point where the chamber diameter begins to decrease.

This paper exploits the De Laval nozzle, a convergent-divergent nozzle invented by Carl De Laval toward the end of the 19th century, and it tries to give a practical procedure to design the nozzle of minimum length. The basic assumption made is that the boundary layer thickness is small compared to the characteristic length, i.e. nozzle radius, so that the nozzle flow field can be treated as inviscid for the purpose of designing the aerodynamic lines. Once the aerodynamic lines are determined, a correction can be made to account for the displacement thickness of the boundary layer. This second step of the designing procedure is not treated in here. This basic procedure has been applied successfully to many supersonic nozzles.

1 Introduction

A De Laval nozzle comprises a combustion chamber, a convergent section, a throat and a divergent section. The combustion chamber is a region of high pressure where a chemical combustion or a nuclear reaction releases the energy which in turn increases the enthalpy of the contained fluid. The enthalpy of the fluid is then transformed in kinetic energy by the nozzle. In the convergent section the flow is accelerated from low subsonic conditions, typical of the combustion chamber, to sonic conditions at the throat. In the divergent section the flow is still accelerated from sonic conditions to supersonic conditions. As far as the divergent section design is concerned, a conical linear nozzle with half opening angle of about 15° usually represents a reasonable good compromise between ease of construction (and of mesh generation for the numerical simulations) and thrust loss reduction. A more accurate design would lead to the typical bell-shaped divergent section. This will be discussed in section 3.

The convergent section is usually easier. Typically, any converging shape does accelerates the flow to the required sonic conditions at the throat.

Finally the nozzle design must satisfy an overall relation between the nozzle throat area, the mass flow rate, the stagnation temperature and pressure which can be written, under the assumption of isentropic flow, as follows:

$$\frac{\dot{m}}{A^*} = \frac{p_{st}\sqrt{\gamma}}{\sqrt{RT_{st}}} \left(\frac{2}{\gamma + 1} \right)^{\frac{\gamma+1}{2(\gamma-1)}}$$

2 Convergent Section Design

Two different approaches have been developed in the following sections in order to find the geometry of the convergent section. In the first approach the geometry is computed by assuming a smooth pressure gradient along its axis. In the latter the geometry is obtained in a graphical way by drawing a convergent section with smooth bend variations.

2.1 Pressure Gradient Criterion

The goal of this approach is to obtain a smooth pressure transition from the value at the combustion chamber, i.e. the stagnation pressure, to the value at the throat in order to ensure a flow free of vortices and instabilities. To this end, a design procedure has been developed, based on the quasi-1D gas dynamics relations for flows in variable-area ducts. Exact formulas are valid for a calorically and thermally perfect gas, but they can be used, with reasonable approximation, for non ideal gases as well. The equation which gives the ratio of the unknown variable area distribution along the nozzle axis to the throat area as a function of the Mach number distribution is [2]¹:

$$\left(\frac{A(x)}{A^*}\right)^2 = \frac{1}{M^2(x)} \left[\frac{2}{\gamma + 1} \left(1 + \frac{\gamma - 1}{2} M^2(x) \right) \right]^{\frac{\gamma+1}{\gamma-1}}$$

or:

$$\frac{A(x)}{A^*} = \frac{1}{M(x)} \left[\frac{2}{\gamma + 1} \left(1 + \frac{\gamma - 1}{2} M^2(x) \right) \right]^{\frac{\gamma+1}{2(\gamma-1)}} \quad (1)$$

being $A(x)$ and $M(x)$ the area and the Mach number along the nozzle axis x . From the total temperature conservation law and from the isentropic relation between pressure and temperature, it can be obtained:

$$\frac{p(x)}{p_{tot}} = \left(1 + \frac{\gamma - 1}{2} M(x)^2 \right)^{-\frac{\gamma}{\gamma-1}} \quad (2)$$

being $p(x)$ the pressure along the nozzle axis x . Finally by inverting equation 1:

$$\frac{2}{\gamma + 1} \left(1 + \frac{\gamma - 1}{2} M(x)^2 \right)^{(\gamma+1)} - \left[\frac{A(x)}{A^*} M \right]^{2(\gamma-1)} = 0 \quad (3)$$

The design procedure can be summarized as follows:

¹Equation 5.20

1. An arbitrary Mach number distribution along the nozzle axis, $M(x)$, is chosen;
2. The corresponding pressure distribution is derived from equation 2 ;
3. The first two steps are repeated until a "good" pressure distribution has been found;
4. The area distribution, which gives the shape of the nozzle convergent section, is obtained from equation 1;
5. The designed nozzle is connected to the combustion chamber through a fillet curve;
6. The new pressure distribution is computed by solving equation 3 via Newton method;
7. A check is made that the pressure distribution connected to the new geometry maintains the desired smoothness.

A reasonable choice, for the arbitrary Mach number distribution, can be a generic second order curve:

$$M(x) = a \left(\frac{x}{L} \right)^2 + b \left(\frac{x}{L} \right) + c \quad (4)$$

where L is the convergent section length, with the following boundary conditions:

$$\begin{aligned} M(0) &= 0 & \text{at } x = 0 &= \text{End of the combustion chamber} \\ M(1) &= 1 & \text{at } x = L &= \text{Nozzle throat} \end{aligned}$$

which give the requirements: $c = 0$, $a + b = 1$.

Figure 1 shows three possible choices for the two coefficients a and b and the corresponding pressure curves. The distribution corresponding to a linear shape convergent section is also added to the figure, though it does not fit the second order expression for the Mach number distribution. The linear shape is presented because it often represents a "good", as well as easy, choice. However, as it can be seen in the figure, for an arbitrary chosen overall area ratio of 1322, (combustion chamber radius 0.2m, throat radius 0.0055m), the linear shape generates a very steep pressure gradient.

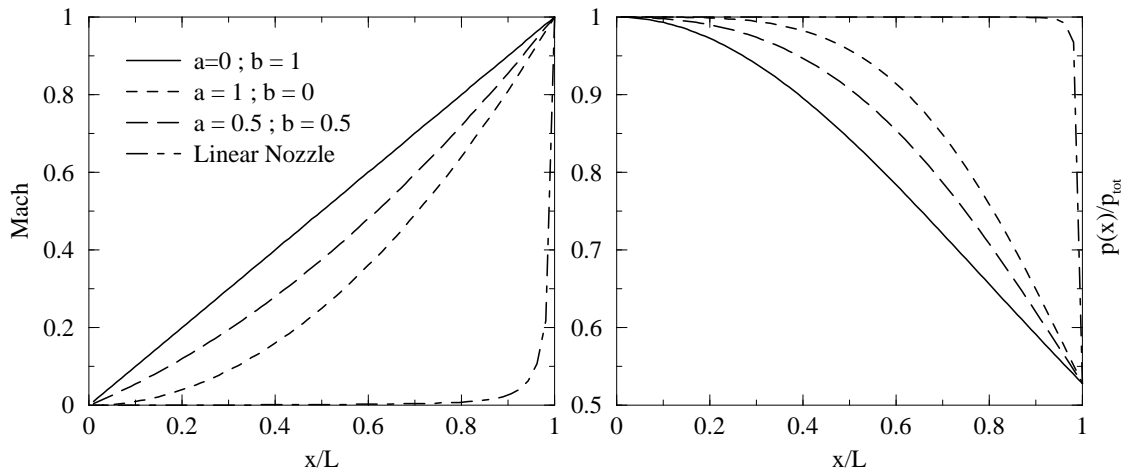


Figure 1: Mach number distributions (left) and corresponding pressure distributions (right).

2.2 Geometric Shape Criterion

According to this approach a “good looking” convergent section shape is chosen and the corresponding pressure distribution is computed. What is meant here by the words “good looking” is a smooth variation of the cross section area from the combustion chamber down to the throat. An easy way to accomplish that is shown in figure 2.

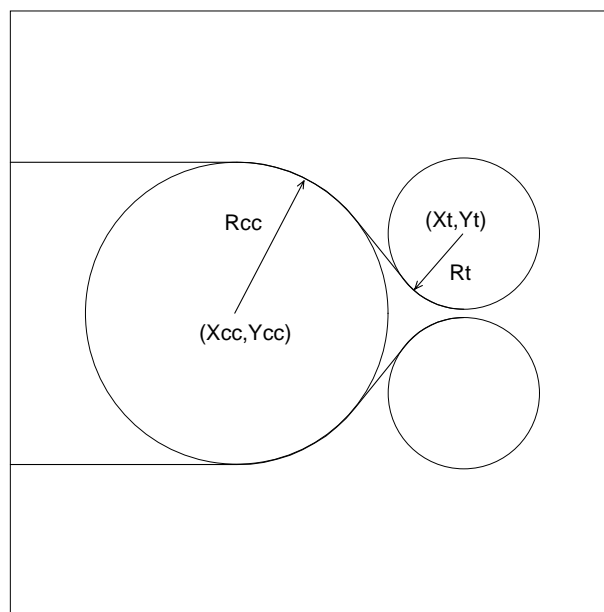


Figure 2: Geometric creation of the convergent section profile

Two circles of given radii have been drawn, one at the end of the combustion chamber and the other at the throat section, together with a line which is tangent to both. The line and the two arcs form the convergent section shape. Four parameters have to be set to fully define the geometry namely the position and the radius of the two circles.

Figures 3 and 4 show the results obtained by varying the distance between the circles while the figures 5 and 6 display the effect of the throat circle radius on the geometry and pressure distribution.

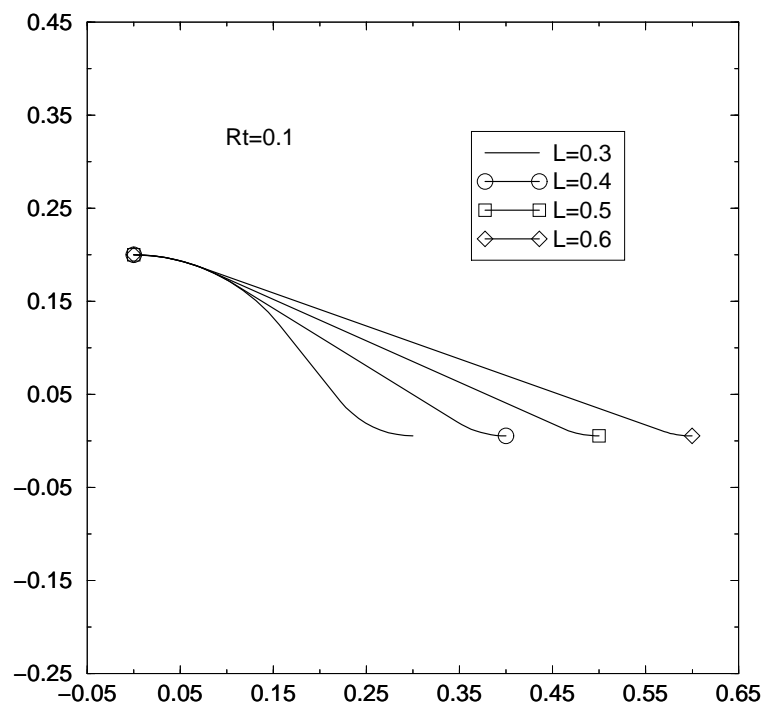


Figure 3: *Effect of L, distance between circles centers on geometry*

It can be seen that the effect of widening the gap between the two circles is, geometrically, to straighten out the convergent section shape and, from the pressure point of view, to reduce the zone where the whole pressure changes take place and as a consequence it causes a steeper pressure curve.

Once have been set the distance between the circles and the combustion chamber circle radius, increasing the throat circle radius has the effect of giving a much rounder shape curve and enlarging the area where the most of the pressure changes takes place this way it reduces the steepness of the pressure curve.

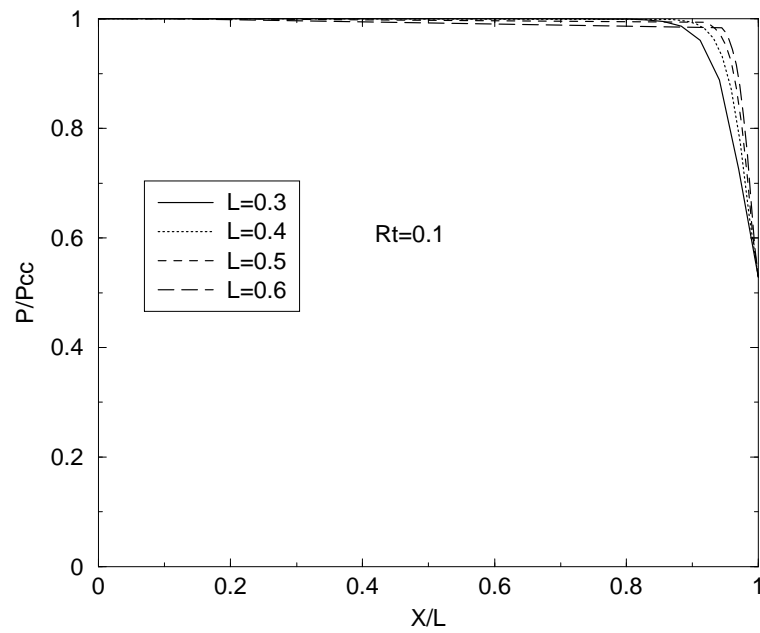


Figure 4: *Effect of L , distance between circles centers on pressure distribution*

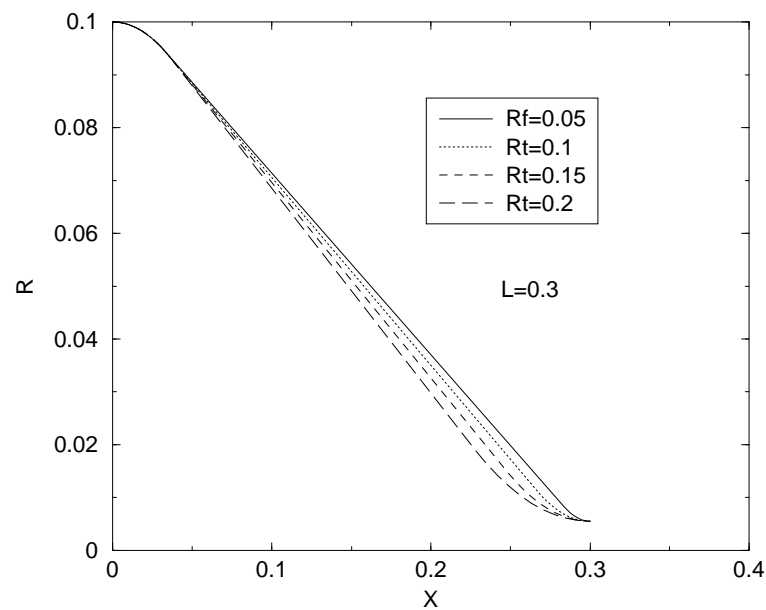


Figure 5: *Effect of Rt , throat circle radius on geometry*

2.3 Conclusions

Comparing the pressure distributions, given by the two criteria, it can be noted that the pressure gradient criterion, for its embedded nature, behaves better; the

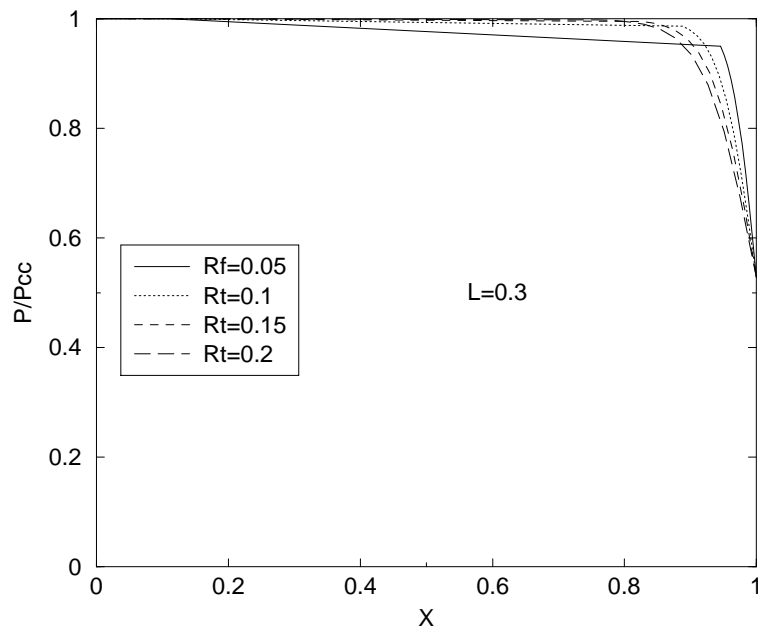


Figure 6: *Effect of R_t , throat circle radius on pressure distribution*

pressure decreases with smoothness to its throat value whereas in the geometric shape criterion there are narrow zones of steep variation and wide zones of constant values.

Figure 7 shows (on the right) the nozzle shape for the pressure gradient criterion with $a = 1$ and $b = 0$ together with the CAD curve connecting the area profile to the stagnation chamber. On the left side of the same figure the two pressure distributions are shown (with and without the connection). The smooth fillet connection generated with a CAD curve does not change the pressure distribution chosen.

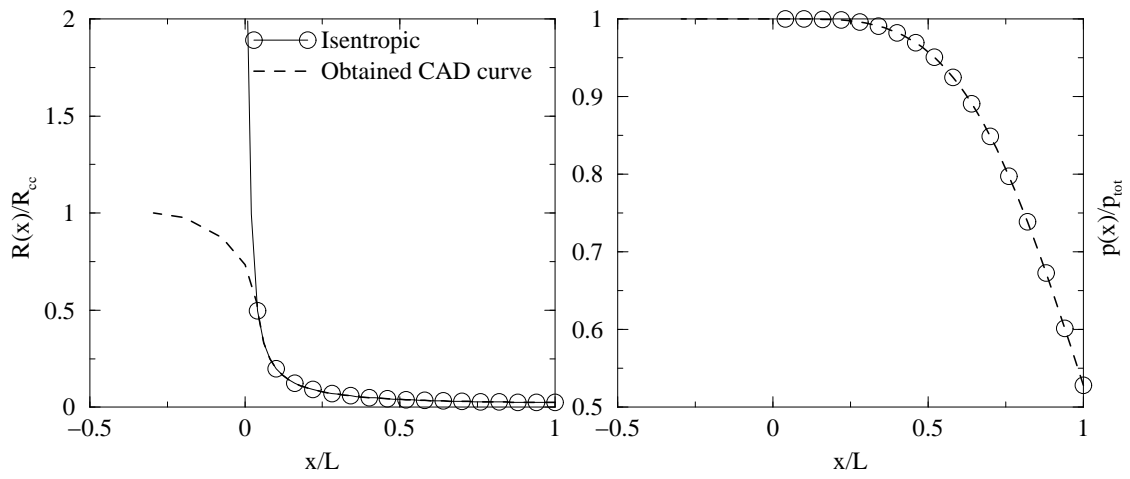


Figure 7: Radius ratio (left) and pressure ratio (right) versus the non dimensional axial coordinate.

3 Divergent Section Design

The effectiveness of a De Laval nozzle design is determined predominantly by the shape of its divergent section. The calculation of the isentropic divergent section, when the effects of thermal transfer and viscous force at the wall are ignored, can be accomplished by using the method of characteristics. The method of characteristics is a well known, simple method for determining the flow inside of a given set of walls; however, the inverse problem, i.e. the determination of an axisymmetric wall contour which gives a particular flow pattern to arbitrary precision, is not as straightforward.

The mathematical utility of the characteristics is that along them the partial differential equations for the flow properties, that is the Euler equations under the assumption of inviscid and adiabatic conditions, are transformed into ordinary differential equations. Physically, they describe the way a disturbance, such as a change in wall angle, propagates through a flowing field. The wall curvature can be approximated by a series of sharp wall bends from which depart the characteristics with their information on the wall angle variation. Recognizing that there is another wall opposite this one with opposite curvature, it is clear that characteristics from the two wall must cross. The result is a sum of effects, and both in two-dimensional and axisymmetric case the axis line can be considered as a symmetry axis and therefore the computation can be limited to one half of the domain (one half of a slice for the axisymmetric case).

For a De Laval nozzle the design aims to reduce all the expansion lines so that at the exit the flow will continue to be uniform to tackle the so called geometry loss.² The procedure for removing or canceling the expansion effects is to accommodate the wall shape in such a way that the incident characteristic will be deflected parallel to the centerline or axis of the nozzle. This procedure is repeated until every characteristic originated in the initial section is removed from the flow.

A generic nozzle divergent section is drawn in figure 8. Half a nozzle is represented for symmetry reasons. \overline{TB} is the throat section and \overline{EF} is the exit section. Let ϑ_{wall} be the angle of the divergent section wall with respect to the centerline. The section of the nozzle where ϑ_{wall} is increasing is called the expansion zone; here expansion waves are generated and propagate downstream, reflecting at the opposite wall. Point C is an inflection point of the contour, where $\vartheta_{wall} = \vartheta_{wall_{max}}$. Downstream of point C, ϑ_{wall} decreases until the wall becomes parallel to the centerline direction. The section from C to E is called the cancelation zone and it is a straightening section

²In fact for conventional bell nozzle, loss mechanism fall into three categories:geometric or divergence loss, viscous drag loss and chemical kinetic loss. Geometric loss results when a portion of the nozzle exit flow is directed away from the nozzle axis, resulting in a radial component of momentum. The second cause of loss depends on the viscous forces while the chemical kinetic loss relies essentially on the fact that the gas is not in chemical equilibrium at any point in the nozzle flow.

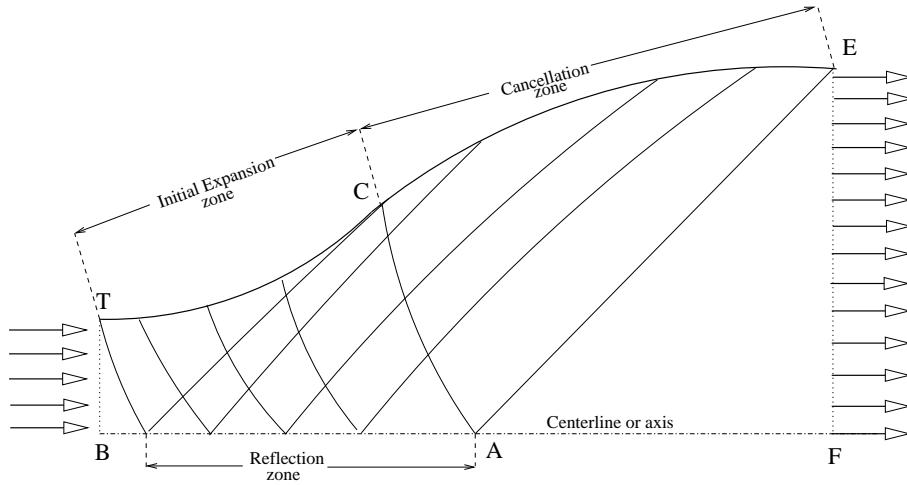


Figure 8: Nozzle divergent section

specifically designed to cancel all the expansion waves generated by the expansion zone. The area TCAB covered with both left- and right-running characteristics is called a non-simple region. In this region the characteristics are curved lines. In contrast, the region CAE is covered by waves of only one family because the other family is canceled. This is called a simple region.

The length and shape of the initial expansion zone are arbitrary. The shortest nozzle, in which this paper is interested, is obtained by having zero length for the initial expansion, that is, a Prandtl-Meyer expansion to ϑ_{max} . T collapses into C and all the characteristics depart from the same point.

Any point of the flow field along a characteristic is described by two variables: the angle ϑ of the velocity with respect to the centerline and ν , the Prandtl-Meyer function which is defined as:

$$\nu = \sqrt{\frac{\gamma + 1}{\gamma - 1}} \arctan \sqrt{\frac{\gamma - 1}{\gamma + 1} (M^2 - 1)} - \arctan \sqrt{M^2 - 1}$$

Thus a supersonic Mach number M is always associated with a definite value of the function ν . As M varies from 1 to ∞ , ν increases monotonically from 0 to ν_{max} .

Figure 9 shows the meaning of the angle ϑ and displays the left- and right-running characteristics at a generic point P. The angle μ between the characteristics and the velocity is called the Mach angle and it is related to the Mach number through the simple relation

$$\sin \mu = \frac{1}{M}$$

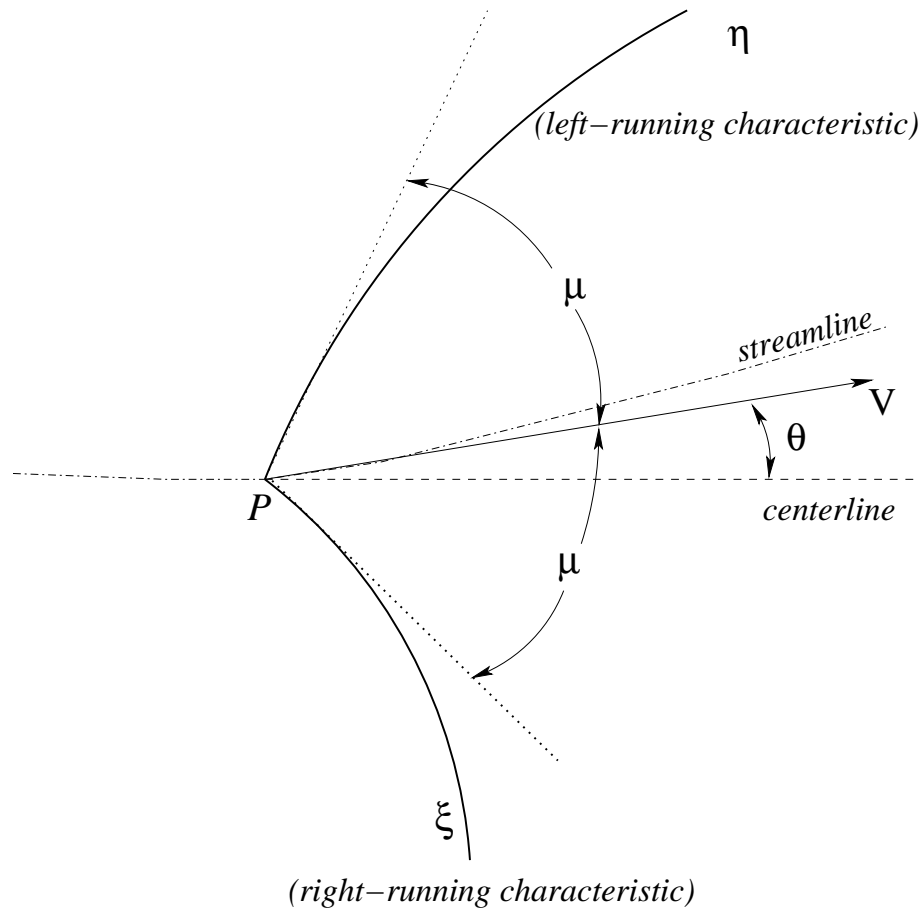


Figure 9: Illustration of left- and right-running characteristics.

3.1 Two-dimensional Divergent Section Design

A relation, called of compatibility, ties the two variables ϑ and ν . By rewriting the equations of motion in the characteristics coordinate system (ξ, η) , after some algebra:

$$\frac{\partial}{\partial \eta} (\nu - \vartheta) = 0$$

$$\frac{\partial}{\partial \xi} (\nu + \vartheta) = 0$$

or:

$$\nu - \vartheta = R = \text{constant along a } \eta - \text{characteristic} \quad (5)$$

$$\nu + \vartheta = Q = \text{constant along a } \xi - \text{characteristic} \quad (6)$$

where Q and R are called the Riemann invariants. The computation method takes advantage of this relation. Figure 10 displays two points where ϑ and ν are known. The position and the variables ϑ and ν in a third, internal, point are obtained.

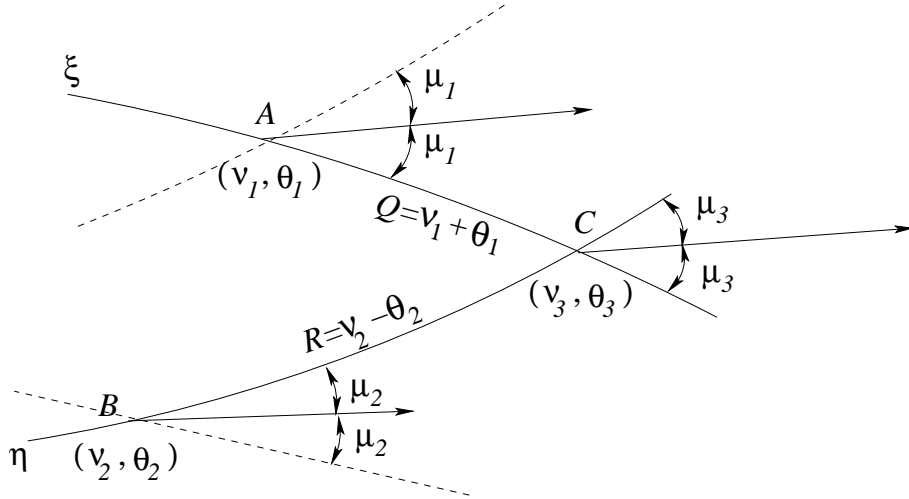


Figure 10: Characteristics network for computation of an internal point.

The point C lies on the crossing of the characteristics passing through the two points A and B . The characteristics are assumed to be straight lines in \overline{AC} and \overline{BC} . Therefore the point C has coordinates:

$$x_3 = \frac{(q_1 - q_2)}{(m_2 - m_1)} \quad (7)$$

$$y_3 = m_1 x_3 + q_1 \quad (8)$$

with:

$$m_1 = \tan(\vartheta_1 - \mu_1)$$

$$q_1 = y_1 - m_1 x_1$$

$$m_2 = \tan(\vartheta_2 + \mu_2)$$

$$q_2 = y_2 - m_2 x_2$$

From the constance of the Riemann invariants, ν_3 and θ_3 are obtained:

$$\nu_3 = \frac{1}{2}(\nu_1 + \nu_2) + \frac{1}{2}(\vartheta_1 - \vartheta_2) \quad (9)$$

$$\vartheta_3 = \frac{1}{2}(\nu_1 - \nu_2) + \frac{1}{2}(\vartheta_1 + \vartheta_2) \quad (10)$$

or in terms of invariants:

$$\nu_3 = \frac{1}{2}(Q + R) \quad (11)$$

$$\vartheta_3 = \frac{1}{2}(Q - R) \quad (12)$$

If the point C lies on the centerline (figure 11) only a right-running characteristic is involved.

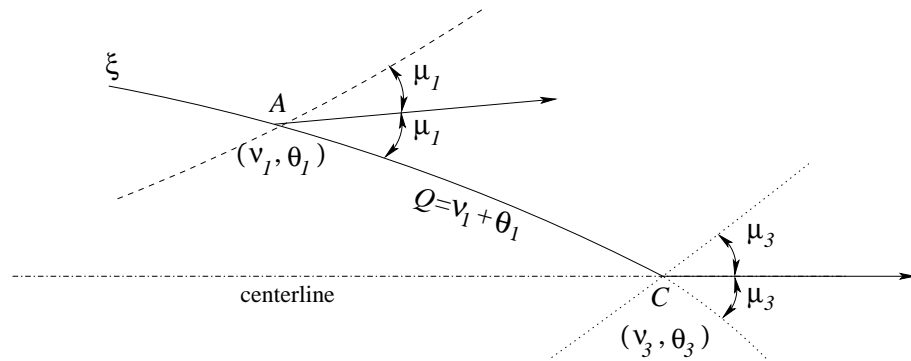


Figure 11: Characteristic network for computation of a centerline point.

The expressions 9 and 10 become:

$$\nu_3 = \nu_1 + \vartheta_1$$

$$\vartheta_3 = 0$$

where the second condition is due to the symmetry of the problem.

If the point C is a wall point then the situation is the one depicted in figure 12. The intersection between the wall contour and the left-running characteristic gives the new boundary point. At the point C $\vartheta = \vartheta_2$ in order to guarantee the cancelation of the expansion wave. From the equation 5 ν is also conserved. In formulas:

$$\nu_3 = \nu_2$$

$$\vartheta_3 = \vartheta_2$$

The wall slope changes to ϑ_3 to let the flow straighten out.

Finally for a two-dimensional nozzle the maximum deflection of the wall contour ϑ_{max} , which occurs at the point of inflection, can be easily calculated from the exit Prandtl-Meyer function:

$$\vartheta_{max} = \frac{\nu_{exit}}{2}$$

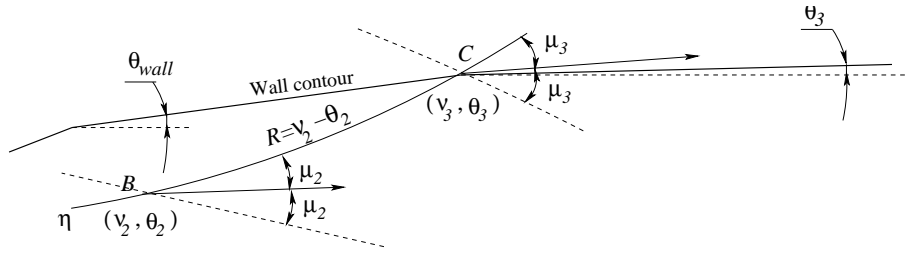


Figure 12: Characteristic network for computation of a boundary point.

3.1.1 Numerical Methods

Two methods are applied in order to obtain the two-dimensional divergent section design namely the method of characteristics and the method of weak waves, usually called method of characteristics as well.

Method of Weak Waves According to the equations 11 and 12, in going along a left-running characteristic, i.e. η , the Riemann invariant R is constant and so the changes in ν and ϑ depend only on the changes in Q , owing to the crossing of the right-running characteristics, i.e. the ξ 's. Thus:

$$\Delta\nu = \frac{1}{2}\Delta Q = \Delta\vartheta$$

Similarly, in going along a right-running characteristic:

$$\Delta\nu = \frac{1}{2}\Delta R = -\Delta\vartheta$$

so a point reached from an initial point P , traversing m left-running characteristics and n right-running characteristics, has:

$$\vartheta = \vartheta_P + (m - n) \Delta\vartheta \quad (13)$$

$$\nu = \nu_P + (m + n) \Delta\vartheta \quad (14)$$

The use of finite weak waves for the construction of plane flows is justified by the theorem that states that the strength of a weak wave is not affected by the intersection with other waves. Here the term strength has the meaning of deflection $\Delta\vartheta$ which the wave produces. On the centerline the strength of the reflected wave is the same as that of the incident one. On the wall the deflection is equal to the strength of the incident wave, which is then canceled.

Referring to figure 13, the method can be outlined as follows:

1. Calculate the ϑ_{max} corresponding to the given M_{exit} ;

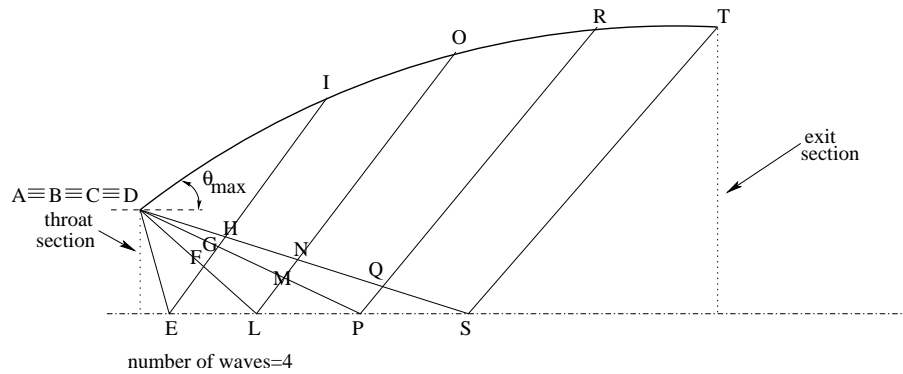


Figure 13: Weak Waves Method.

2. Divide ϑ_{max} by the given number of waves to obtain $\Delta\vartheta$;
3. The waves depart from the throat edge (Points A to D in the example). Each wave is drawn with its reflection and cancelation and at any crossing the Prandtl-Meyer function ν and the flow angle ϑ are calculated with the formulas 13 and 14 with C as a generic point P. The Mach number M and the Mach angle μ are hence derived as well;
4. The coordinates of intersection points between waves, waves and wall, waves and centerline are calculated.

The accuracy is improved by increasing the number of waves. The procedure has been implemented on a Fortran code. At all Mach number a good agreement is found with the area ratios resulting from the quasi-1D relation 1 at page 4.

The Method of Characteristics or MOC This method uses the equations 9 and 10 to propagate, starting from the throat, through the field. The program stops when a wall point assumes the desired exit Mach number. Figure 14 roughly shows the appearance of a calculation web.

The accuracy is improved by increasing the number of points if the initial data are reliable. Good initial data are given by a previous Euler computation which can yield the sonic line shape. In order to overcome this problem an effective approach is to accumulate the points near the corner edge and to assign $\nu_1 = \vartheta_1 = \vartheta_{max}$ to the first and: $\nu_i = \vartheta_i = \vartheta_{min} + i \frac{(\vartheta_{max} - \vartheta_{min})}{n-1}$ to the i -th, where ϑ_{min} is an ϵ necessary to avoid numerical problems in the determination of the points and n is the number of points.

The procedure has been implemented and the results are, alike the method of waves, in good agreement with the quasi-1D relation 1 of page 4.

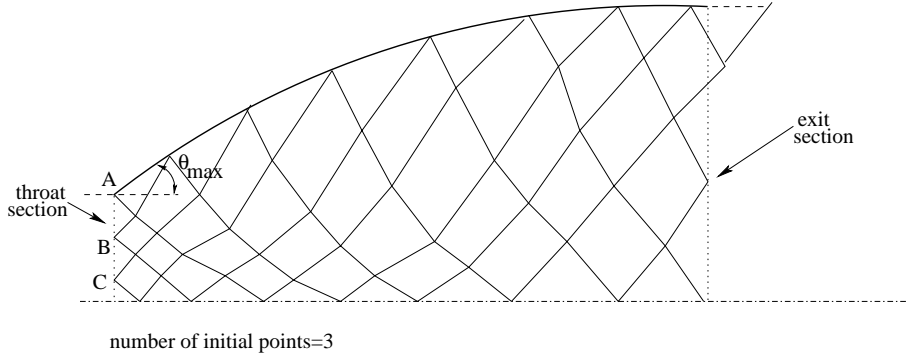


Figure 14: Characteristics Method.

3.2 Axisymmetric Divergent Section Design

The compatibility relation between ϑ and ν assumes a more complicated form than the corresponding two-dimensional, because the geometry of the flow field is now involved through the variable r , distance from the centerline:

$$\frac{\partial(\nu - \vartheta)}{\partial\eta} = \frac{\sin\mu \sin\vartheta}{r} \quad (15)$$

$$\frac{\partial(\nu + \vartheta)}{\partial\xi} = \frac{\sin\mu \sin\vartheta}{r} \quad (16)$$

Two methods for solving the equations 15 and 16 are here presented. The first one [5] is to write them in a finite difference form. The latter [1] is to approximate them.

Developing the first approach the two equations, which are valid along the left- and right-running characteristic respectively, are

$$\Delta\vartheta = A \Delta M - B \Delta x \quad (17)$$

$$\Delta\vartheta = -A \Delta M + C \Delta x \quad (18)$$

where x is the centerline axis coordinates originated on the throat and the coefficients are in turn given by

$$A = \frac{\sqrt{M^2 - 1}}{M \left(1 + \frac{\gamma-1}{2} M^2\right)}$$

$$B = \frac{1}{\left(\sqrt{M^2 - 1} \cot\vartheta - 1\right) r}$$

$$C = \frac{1}{\left(\sqrt{M^2 - 1} \cot\vartheta + 1\right) r}$$

In order to compute the coordinates and the flow variables on a third point, given the coordinates and flow data on the first two, the use of an iterative procedure is necessary. The formulas for the coordinates of the third point are the equations 7 and 8, same as the two-dimensional case, while M_3 and ϑ_3 are obtained from:

$$M_3 = \frac{\vartheta_1 - \vartheta_2 + A_1 M_1 + A_2 M_2 + B_2 (x_3 - x_2) + C_1 (x_3 - x_1)}{A_1 + A_2} \quad (19)$$

$$\vartheta_3 = \vartheta_2 + A_2 (M_3 - M_2) - B_2 (x_3 - x_2) \quad (20)$$

When the distance r is null, it can be shown that the 18 takes the following form:

$$\Delta\vartheta = \frac{1}{2} A \Delta M$$

The second approach, see figure 15, integrates the equations 15 along the characteristic segments AC and BC:

$$\int_2^3 d(\nu - \vartheta) = \int_2^3 \left(\frac{\sin \mu \sin \vartheta}{r} \right) d\eta$$

$$\int_1^3 d(\nu + \vartheta) = \int_1^3 \left(\frac{\sin \mu \sin \vartheta}{r} \right) d\xi$$

Assuming the quantities in parentheses on the right-hand side to be constant over the interval of integration, the integration leads to:

$$\nu_3 - \vartheta_3 = \nu_2 - \vartheta_2 + \frac{\sin \mu_2 \sin \vartheta_2}{r_2} \Delta\eta_{23} \quad (21)$$

$$\nu_3 + \vartheta_3 = \nu_1 + \vartheta_1 + \frac{\sin \mu_1 \sin \vartheta_1}{r_1} \Delta\xi_{13} \quad (22)$$

where $\Delta\eta_{23}$ and $\Delta\xi_{13}$ are the distance from point B to C and from A to C, respectively.

Comparing the equations 5 and 6 with the 21 and 22 it is clear the presence of an additional term dependent on the geometry and on the flow variables. The Riemann invariants are not valid anymore. Solving the equations 21 and 22 for ν_3 and ϑ_3 :

$$\nu_3 = \frac{1}{2} (\nu_1 + \nu_2) + \frac{1}{2} (\vartheta_1 - \vartheta_2) + \frac{1}{2} \left(\frac{\sin \mu_1 \sin \vartheta_1}{r_1} \Delta\xi_{13} + \frac{\sin \mu_2 \sin \vartheta_2}{r_2} \Delta\eta_{23} \right) \quad (23)$$

$$\vartheta_3 = \frac{1}{2} (\nu_1 - \nu_2) + \frac{1}{2} (\vartheta_1 + \vartheta_2) + \frac{1}{2} \left(\frac{\sin \mu_1 \sin \vartheta_1}{r_1} \Delta\xi_{13} - \frac{\sin \mu_2 \sin \vartheta_2}{r_2} \Delta\eta_{23} \right) \quad (24)$$

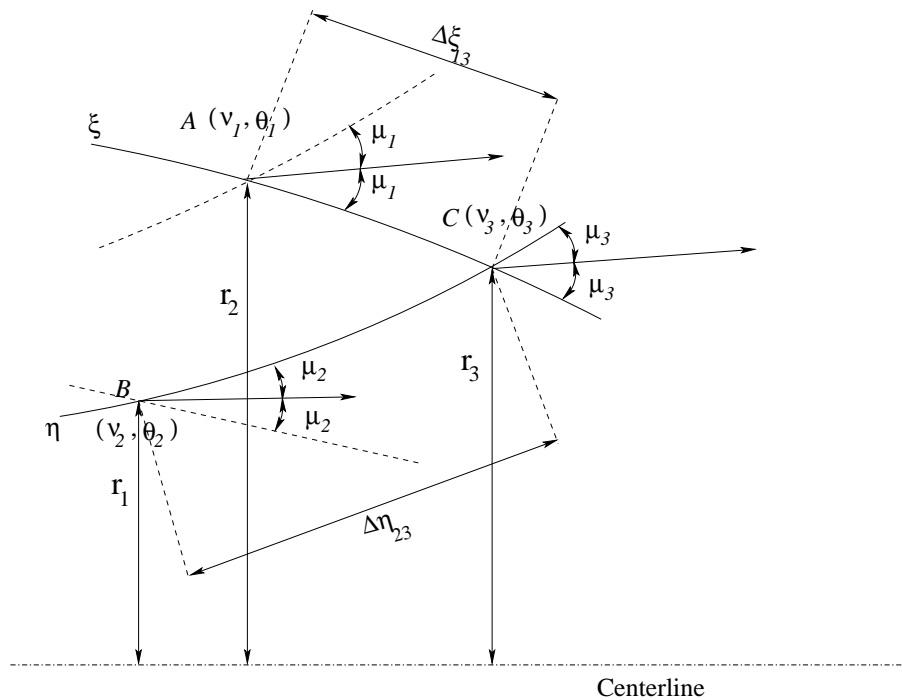


Figure 15: Characteristics network for computation of an internal point.

which are the equivalent of the 9 and 10 for the axisymmetric case.

If the point C lie on the centerline only a right-running characteristic is involved.

The expressions 23 and 24 become:

$$\begin{aligned} \nu_3 &= \nu_1 + \vartheta_1 + \frac{\sin \mu_1 \sin \vartheta_1}{r_1} \Delta \xi_{13} \\ \vartheta_3 &= 0 \end{aligned}$$

where the second expression is due to the symmetry of the problem.

If the point C is a wall point, its coordinates are given by the intersection between the wall contour and the left-running characteristic. The point C has $\vartheta_3 = \vartheta_2$ in order to cancel the incident wave. The characteristic doesn't encounter any other characteristic so the ν is also conserved. In formulas:

$$\begin{aligned} \nu_3 &= \nu_2 \\ \vartheta_3 &= \vartheta_2 \end{aligned}$$

The wall slope assumes the value ϑ_3 to let the flow straighten out.

The maximum deflection of the wall contour ϑ_{max} cannot be easily calculated. So, for a minimum length nozzle, it is a result of the numerical solution.

3.2.1 Numerical Methods

The same methods seen in section 3.1.1 are usable with some adjustments.

Method of Weak Waves With respect to the two-dimensional case, ϑ_{max} is not known in advance and the wave strength depends on the characteristic network geometry. That leads to the following procedure (see figure 13) :

1. Guess a ϑ_{max} ;
2. Divide ϑ_{max} by the given number of waves to obtain $\Delta\vartheta$ which is now used only to define the strength of the initial points (Points A,B,C,D in the example);
3. The waves depart from those points. Each wave is drawn with its reflection and cancelation and, at any crossing, the Prandtl-Meyer function ν and the flow angle ϑ are calculated, with the formulas 22, together with the coordinates x_3 and y_3 . The Mach number M and the Mach angle μ are hence derived as well;
4. Compare ν_T to $\nu_{exit\ desired}$ and modify the ϑ_{max} accordingly. Return to step 2.

The method has been implemented and the area ratios found are significantly smaller than the ones predicted by the quasi-1D relation 1 at page 4.

Method of Characteristics or MOC The method has to be iterative, just like the Weak Waves Method, because ϑ_{max} is unknown before the computation. A way to accomplish the task is to follow the right-running characteristic departing from the throat edge with $\nu = \nu_{max}$ through its reflection on the axis until it crosses again the wall contour. The ν at the wall is then compared to the $\nu_{exit\ desired}$ and the ϑ_{max} varied accordingly. Figure 16 shows the “special characteristic line” along with the others (which depart from the throat edge with $\nu < \nu_{max}$).

This method, which leads to good results in the two-dimensional case, converges only for low exit Mach numbers. A number of changes have been made to overcome this problem but with no real improvement. Table sums up briefly the formulations which have been tested numerically. Each formulation is described by difference from the one which is more similar to, apart for the first one which is wholly portrayed.

3.3 Conclusions

Two methods have been presented for designing the two-dimensional and axisymmetric divergent sections. In two dimensions the methods are comparable. In axisymmetry the MOC method seems to fail maybe due to its need of reliable initial data on the throat line (or the sonic line geometry).

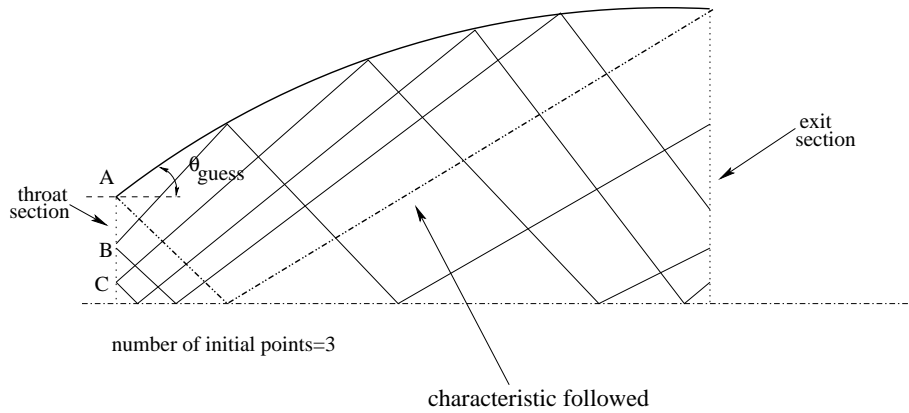


Figure 16: Characteristic Method for axisymmetric nozzle.

#	Similar to #	Description or Difference from the similar one
1	-	Formulation MOC approximated. Points on the throat column equally spaced. External loop which modifies ϑ_{max} based on v_{exit} value. Every loop stops when $v_{wall} > v_{desired}$ or $\vartheta_{wall} < \epsilon$.
2	1	The slope of the characteristics is calculated by averaging the slope of lines AC and BC.
3	1	ϑ_{wall} is taken as the average of the last ϑ_{wall} and the new ϑ_{wall} .
4	1	Points on the throat are distributed according to a cosine law.
5	4	The integral is obtained by averaging $\sin \vartheta, \sin \mu$ and r between AC, and BC
6	4	The check to exit from the loop is made on the characteristic line at v_{max}
7	6	$\frac{1}{r} dv$ and $\frac{1}{r} d\eta$ are integrated
8	6	The integral is obtained by averaging $\sin \theta, \sin \mu$ and r between AC and BC.
9	6	Points on the column are divided in a part equally spaced and in a part distributed with cosine law
10	9	Finite Difference formulation only for the points on the centerline.
11	9	Finite Differences formulation for all the points.
12	11	The points distributed with cos law are made coincident to the throat edge.
13	12	$v_{wall} = v_{internal}$ for any wall points.
14	12	The mass flow conservation is used to place the points on the wall.
15	12	The point C is obtained through iterations.
16	15	The mass flow conservation is used to place the points on the wall.
17	12	The formulation is changed to the MOC approximated.

Table 1: Summary of formulations tested numerically.

4 Results

In order to verify the quality of the design procedure a test has been carried out on three axisymmetric rocket nozzles. The first nozzle is designed with the convergent and divergent sections geometry deriving by the application of the pressure gradient criterion and the weak waves method. The second nozzle has the same convergent of the first nozzle but the divergent contour is a straight line³. Finally the third nozzle has both convergent and divergent section contours drawn as straight lines. The nozzles all have the same radius at the combustion chamber, at the throat and at the exit section and the same convergent and divergent section lengths. The three nozzles hereafter will be referred to as the “condiv” nozzle, the “convlin” nozzle and the “linear” nozzle.

The main common design parameters of the nozzles are given in table 2.

Symbol	Meaning	Value
R_{cc}	Combustion Chamber Radius	0.2m
R^*	Throat Radius	0.1m
T_{cc}	Combustion Chamber or Total Temperature	2500K
\dot{m}	Mass Flow Rate	5.0Kg/s
M_E	Exit Mach Number	3.0
R, γ	Specific Gas constant for air, Specific heat ratio for air	287 J/KgK, 1.4

Table 2: Common design parameters of the three nozzles.

The coefficients used in the pressure gradient criterion, see section 2.1 page 4, are $a = 1$ and $b = 0$, which result in a parabolic Mach number distribution along the axis of the convergent section. A convergent section length of $L = 0.2m$ have been chosen.

The divergent section shape is obtained by the application of the method of waves, see section 3.2.1 page 21. With 200 waves, the area ratio⁴ corresponding to the given M_E is approximately

$$\frac{A_E}{A^*} = 3.88$$

so that the exit radius is

$$R_E = 0.196979m$$

³In 2D a straight line. In axisymmetry a frustum of cone.

⁴Area ratio is the cross sectional area of the nozzle exit divided by the cross sectional area of the nozzle throat.

The one-dimensional equation 1 would give $M_E = 2.91$ for the same area ratio, or $\frac{A_E}{A^*} = 4.23$ for the same $M_E = 3.00$.

The combustion chamber pressure or total pressure is given by:

$$P_{cc} = \frac{\dot{m}}{A^*} \sqrt{\frac{RT_{cc}}{\gamma}} \left(\frac{2}{\gamma + 1} \right)^{-\frac{\gamma+1}{2(\gamma-1)}} = 196890 \text{ Pa}$$

The exit static pressure and temperature can be easily obtained from the isentropic relations:

$$P_E = P_{cc} \left(1 + \frac{\gamma - 1}{2} M_E^2 \right)^{-\frac{\gamma}{\gamma-1}} = 5360 \text{ Pa} \quad (25)$$

$$T_E = T_{cc} \left(1 + \frac{\gamma - 1}{2} M_E^2 \right)^{-1} = 892.86 \text{ K} \quad (26)$$

The methods presented earlier in this report are valid under the assumption of inviscid flow hence the test case has been carried out by solving the Euler equation. In addition to the Euler computation a computation has been made using the Navier-Stokes equations plus the Spalart-Allmaras turbulence model, in order to check how the methods behave when the viscosity play a role in the flow evolution.

All the computations have been conducted with the commercial code Fluent release 6.

4.1 Inviscid Computations

The computational grids used are shown in figure 17. The grids are structured and they have 131 points along the axis by 21 points along the radius.

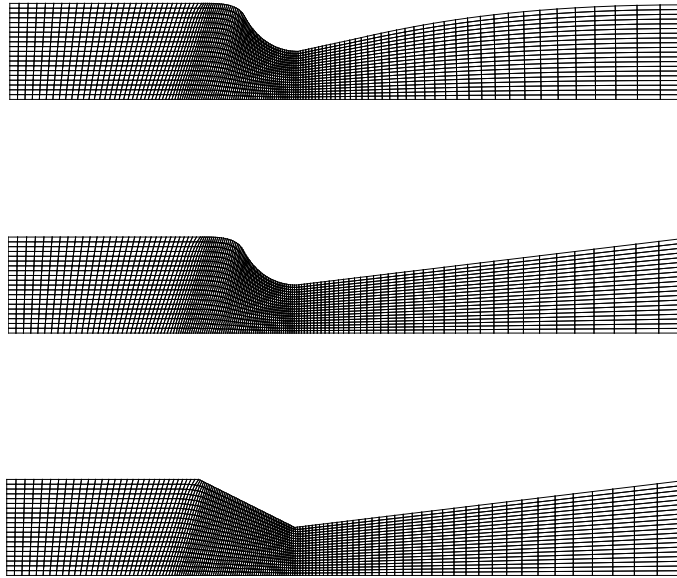


Figure 17: Grids used for the inviscid computations. From top to bottom the condiv nozzle, the convlin nozzle and the linear nozzle.

A summary of the main computational settings used for the calculation is presented in table 3 .

Type of Calculation	Inviscid
Dimension	2D-Axisymmetric
Solver	Coupled - Implicit
Preconditioning	Yes
Discretization	2nd order upwind
Used Boundary Condition	
Inlet	Static Pressure, Total Temperature, Velocity Direction
Wall	Adiabatic Solid Wall
Outlet	Static Pressure while subsonic conditions exist

Table 3: Main Fluent settings.

The convergence histories are reported in figure 18, 19 and 20. The mass flow rate balance error is of order $1.E - 6$ on all grids.

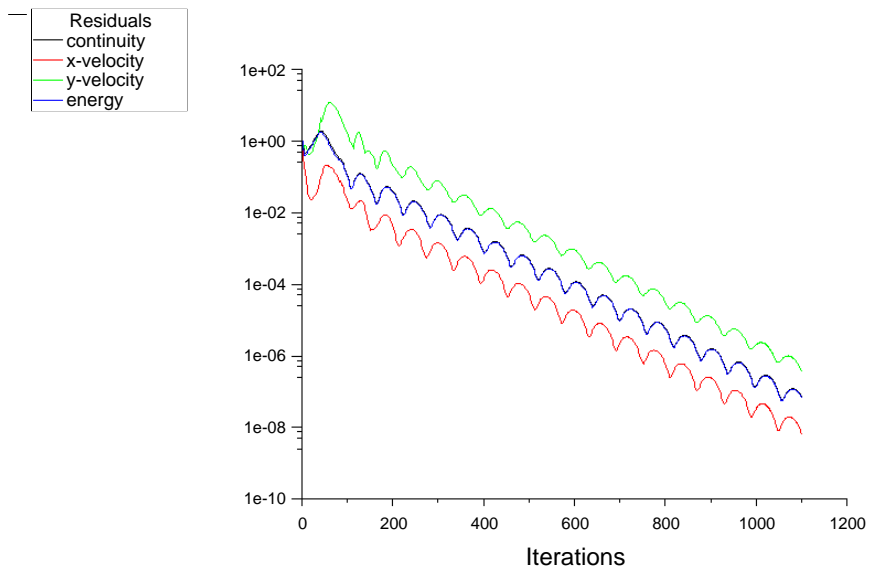


Figure 18: Convergence history of the convdiv nozzle.

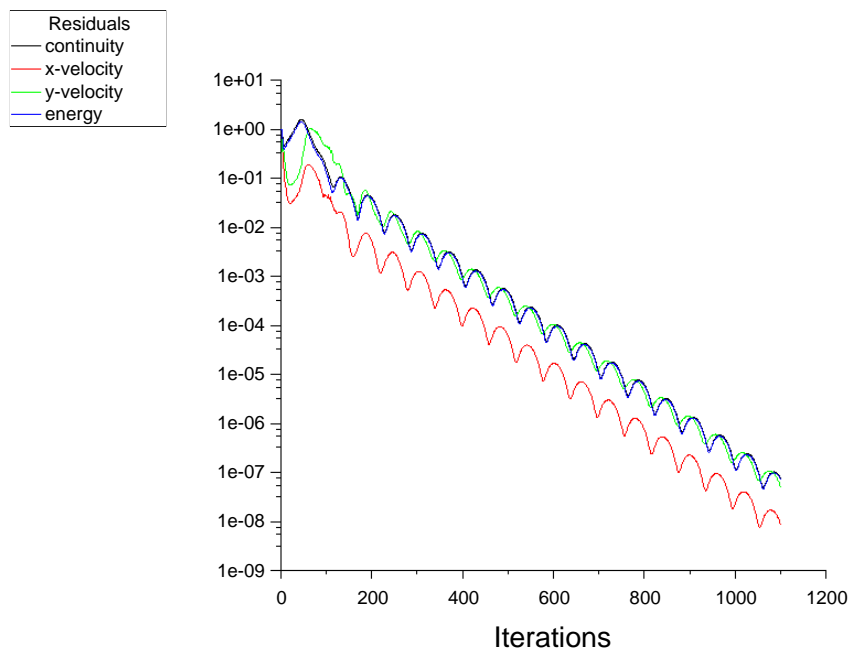


Figure 19: Convergence history of the convlin nozzle.

Figures 21, 22 and 23 show the vector field on the nozzles with the enlargements

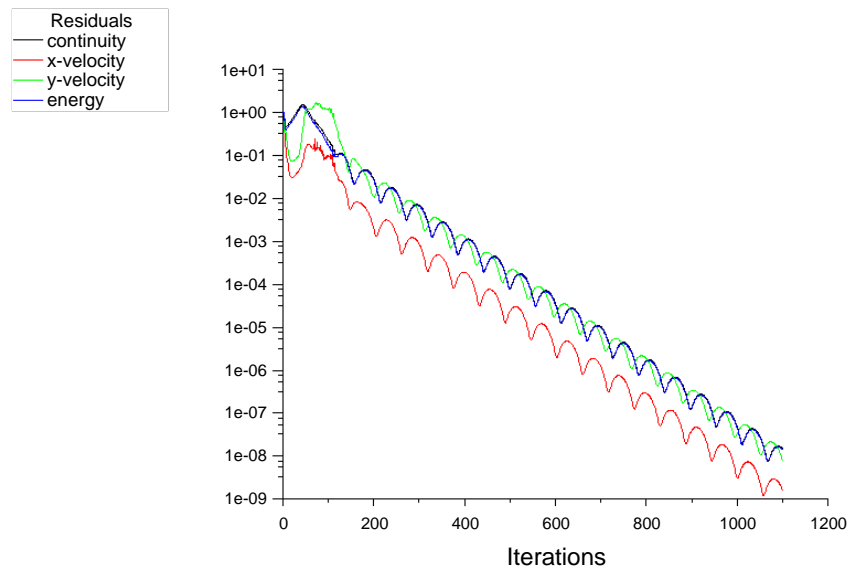


Figure 20: Convergence history of the linear nozzle.

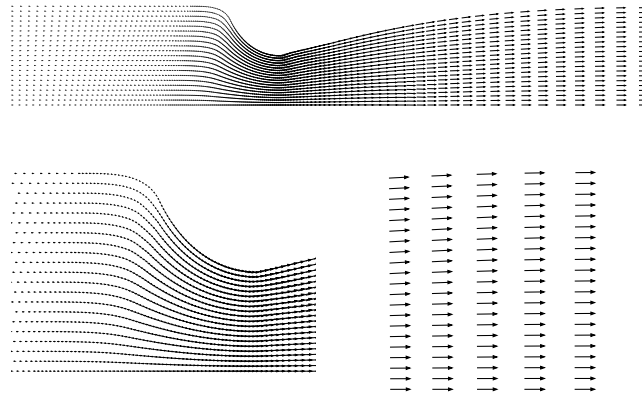


Figure 21: Vectors on the convdiv nozzle.

of the convergent portion and the exit area. Both convergent section shapes seem to give the same flow pattern whereas the flow in divergent sections differs. In fact the convlin and the linear nozzle have, at the exit section, a significant radial component

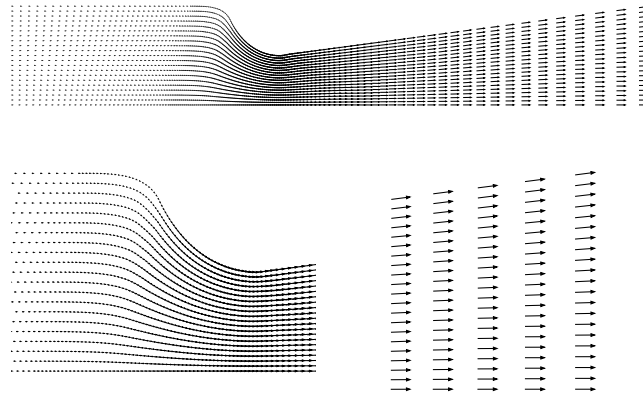


Figure 22: Vectors on the convlin nozzle.

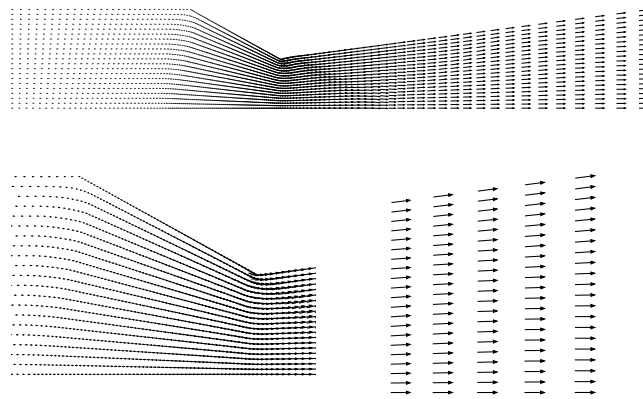


Figure 23: Vectors on the linear nozzle.

of the velocity which causes a net thrust loss.

The Mach number along the nozzle axis is reported in figure 24. The trend along the convergent section is, as imposed, parabolic for both the convdv and convlin nozzles. In the divergent section a sudden drop is registered at an axial coordinate range $0.3 < x < 0.5$. By running the three-dimensional case, see figure 25, the

drop is substituted by a slight change in slope and the Mach behavior in the convdiv nozzle is now increasing monotonic. The three-dimensional grids, figures 32 to 34, are obtained from the rotation of 360° of the axisymmetric grids. The number of points on the circumferential direction is 41.

The Mach number fields for the axisymmetric and 3d grids are drawn in figure 26 and 27. The isolines of the axisymmetric nozzles are irregular even though the convergence has been reached. The worst behavior in terms of Mach number seems to happen near the centerline. This fact may indicate some problem of Fluent with the axis boundary condition in the axisymmetric model.

The three nozzles have a different Mach number isolines appearance. The convdiv nozzle reaches higher Mach numbers at the exit and its isolines are much stretched along the axis direction.

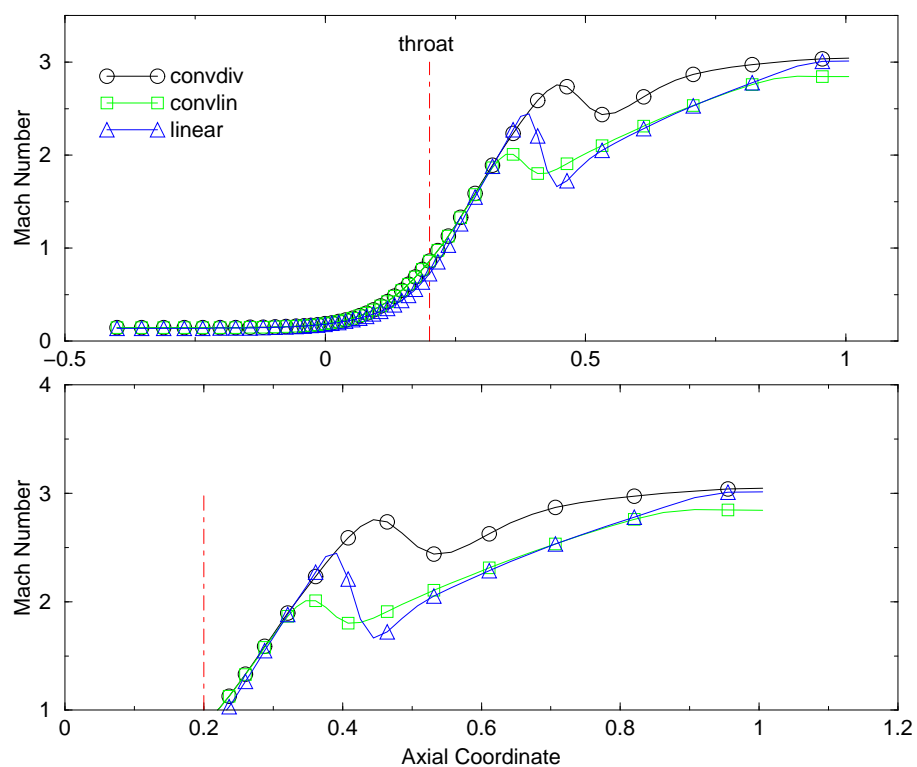


Figure 24: Mach number along the axis line for the three nozzles.

The static temperature behavior depends closely on the Mach number. In figure 28 is reported the static temperature along the axis. The sudden rise in temperature in the divergent section, top of figure 28, is a consequence, via the isentropic relation 26, of the Mach number drop, which has been previously registered.

Figure 29 shows the result obtained with the three-dimensional grids described earlier. Again the trend of the convdiv nozzle is monotonic and its exit value is lower than the other nozzles.

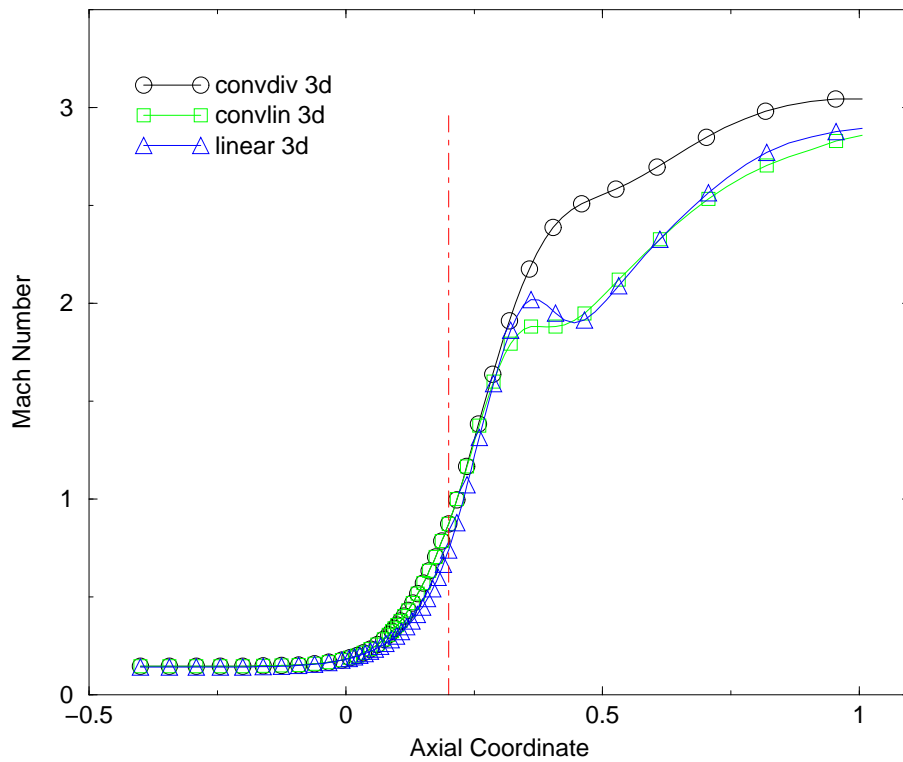


Figure 25: Mach number along the axis line for the three 3d nozzles.

The static pressure along the nozzle axis is displayed in figure 30. The convdiv and convlin nozzles has, with respect to the linear nozzle, a larger zone of pressure variation in the convergent section that is lower pressure gradients. In the divergent section the convdiv is the nozzle which gives a lower exit pressure. The sudden rise in pressure in the divergent section is again a consequence of the Mach distribution. In figure 31 is shown the pressure distribution for the three nozzles computed on the three-dimensional grids.

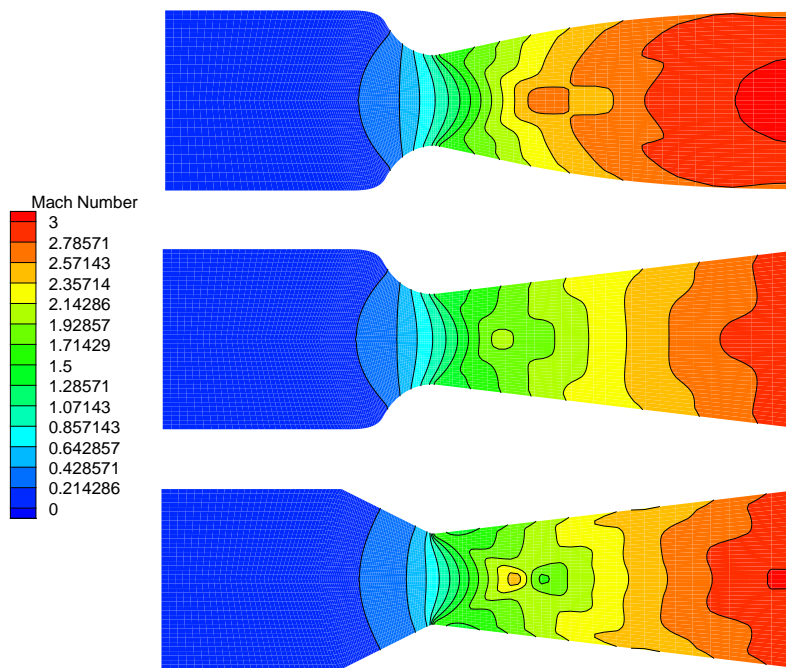


Figure 26: From top to bottom. Mach field for the convdiv, the convlin and the linear nozzles.

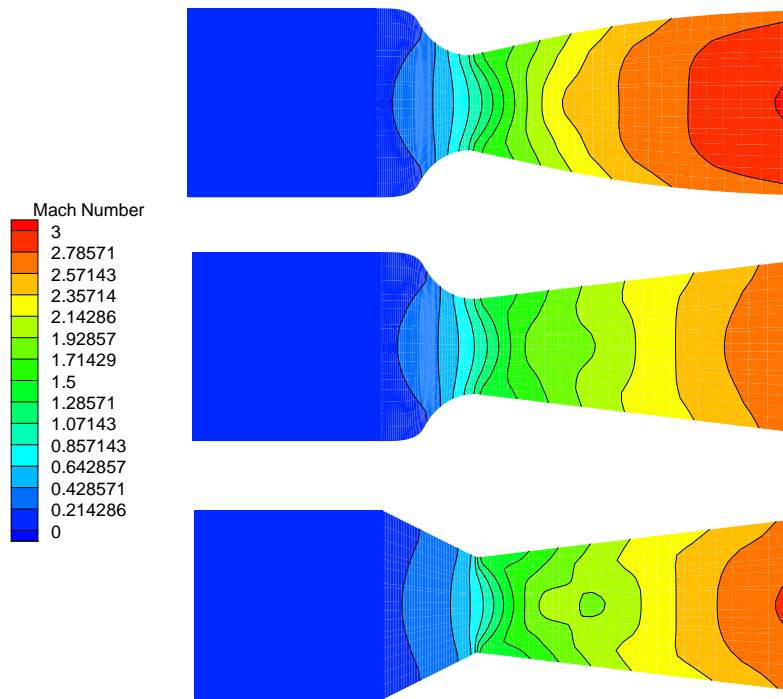


Figure 27: From top to bottom. Mach field for the convdiv 3d, the convlin 3d and the linear 3d nozzles.

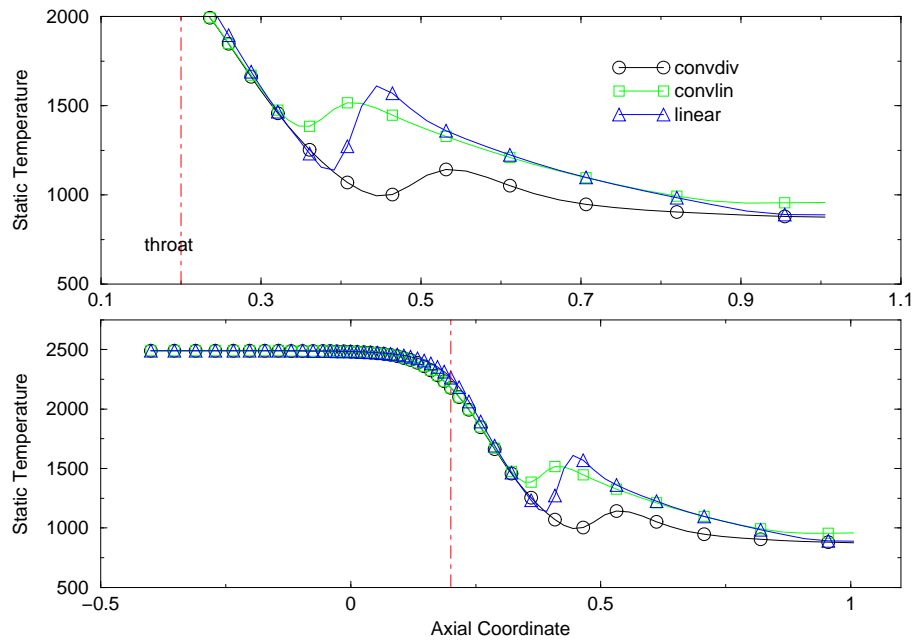


Figure 28: Static temperature for the three nozzles.

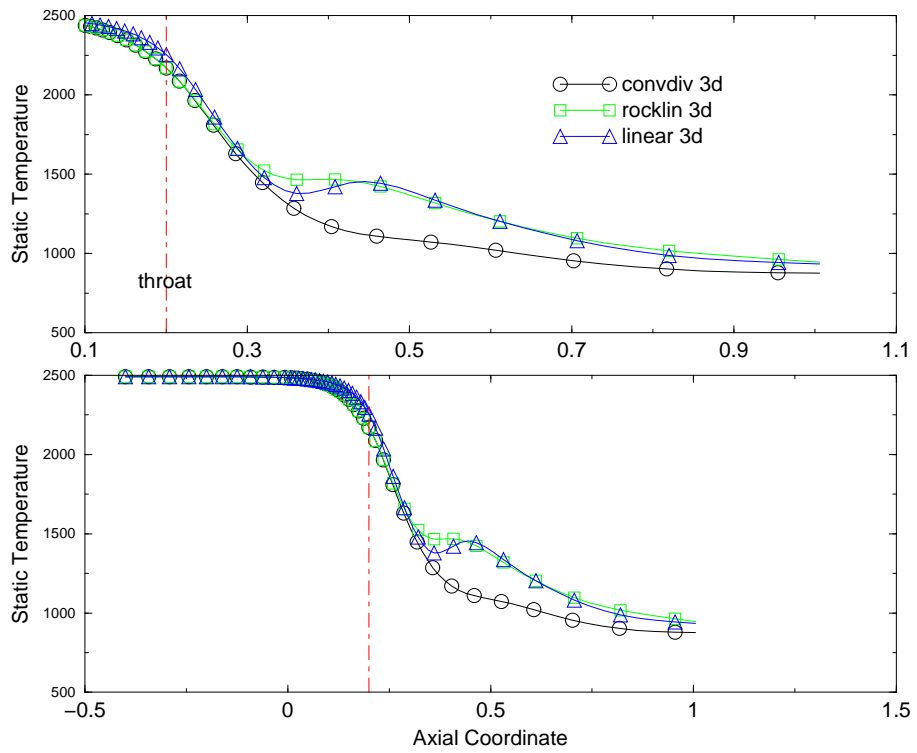


Figure 29: Static Temperature for the three 3d nozzles.

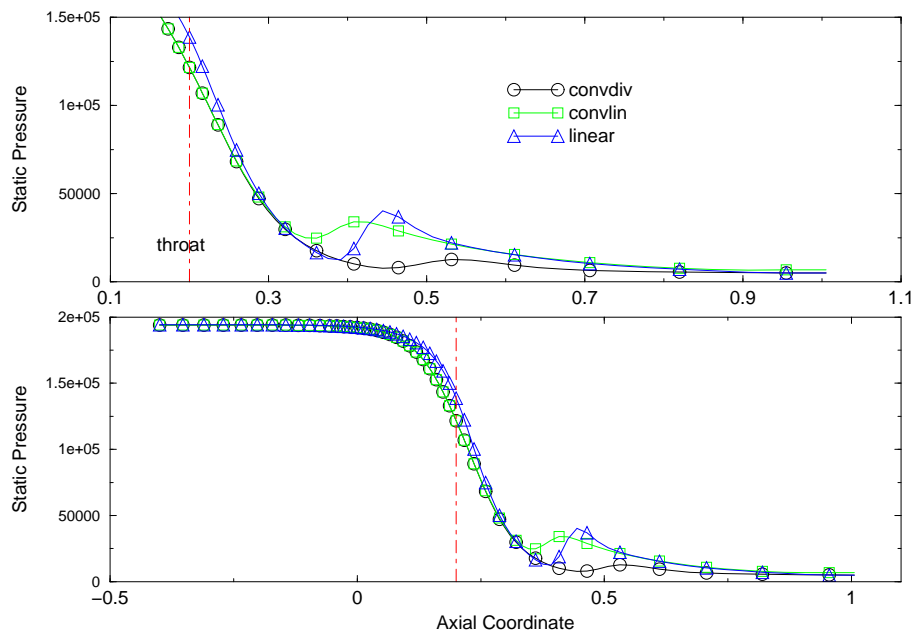


Figure 30: Static pressure for the three nozzles.

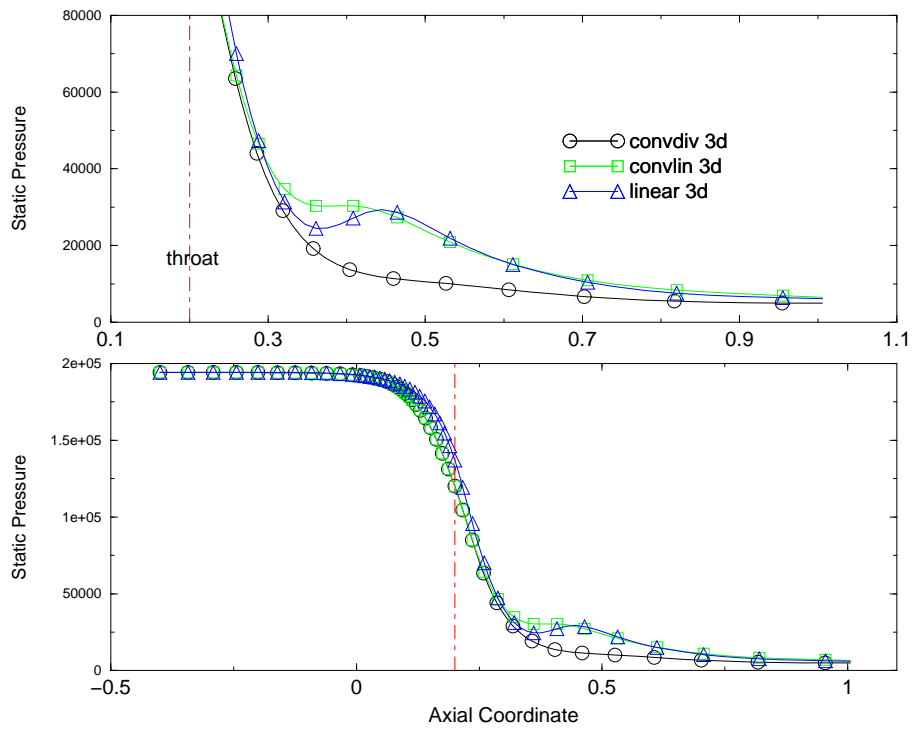


Figure 31: Static Pressure for the three 3d nozzles.

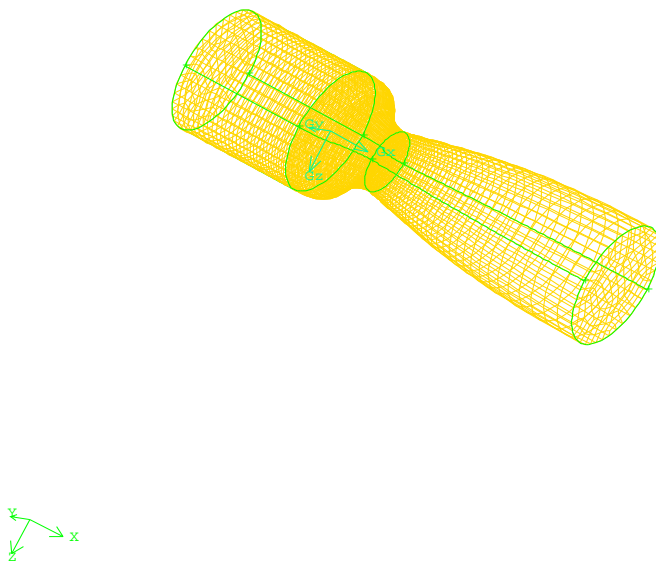


Figure 32: 3D grid on convdiv nozzle.

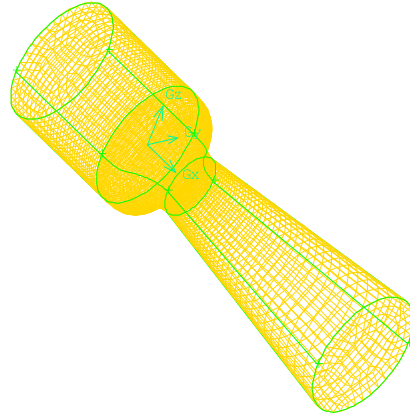


Figure 33: 3D grid on convlin nozzle.

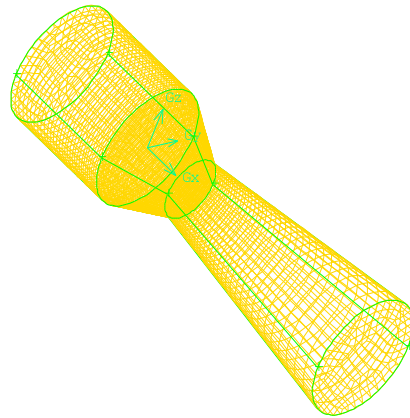


Figure 34: 3D grid on linear nozzle.

4.2 Viscous Computations

In figure 35 are shown the grids used in the computations. The dimensions are 131 points in the axial direction by 60 in the radial direction. The grids are highly stretched in order to capture the boundary layer.

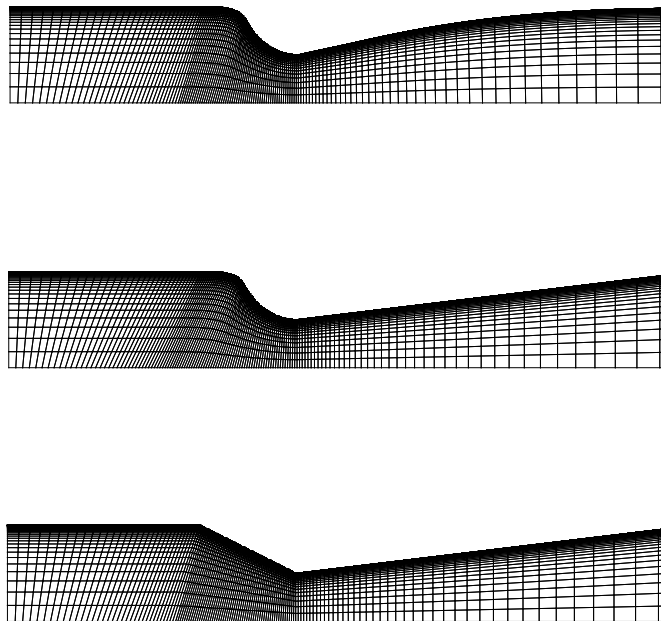


Figure 35: Grids used for the viscous computations. From top to bottom the condiv nozzle, the convlin nozzle and the linear nozzle.

The main computational settings used for the calculation are summarized in table 4. The convergence histories are reported in figure 36, 37 and 38. The mass flow rate balance error is of order $1.E - 4$ on all grids.

Figures 39, 40 and 41 show the vector field on the nozzles with some enlargements. The boundary layer seems to be correctly reproduced. Again only the condiv nozzle has, at the exit section, the vectors aligned along the axial direction.

The Mach number along the nozzle axis is reported in figure 42. With respect to the inviscid computation, the drop in Mach number magnitude is less severe for all the three cases. Figure 43 marks this comparison.

The drop reduction has been investigated in a three-dimensional sector, whose grid is obtained from the rotation of 10 degrees of the axisymmetric grid. The number of points on the circumferential direction is 5. Figure 45 shows the results for the

Type of Calculation Dimension Solver Preconditioning Discretization	Viscous. Spalart-Allmaras turbulence model 2D-Axisymmetric Coupled - Implicit Yes 2nd order upwind
Used Boundary Condition Inlet Wall Outlet	Static Pressure, Total Temperature, Velocity Direction, Turbulent Viscosity Ratio Adiabatic Solid Wall. no slip condition. Static Pressure while subsonic conditions exist Backflow Modified Turbulent Viscosity

Table 4: Main Fluent settings.

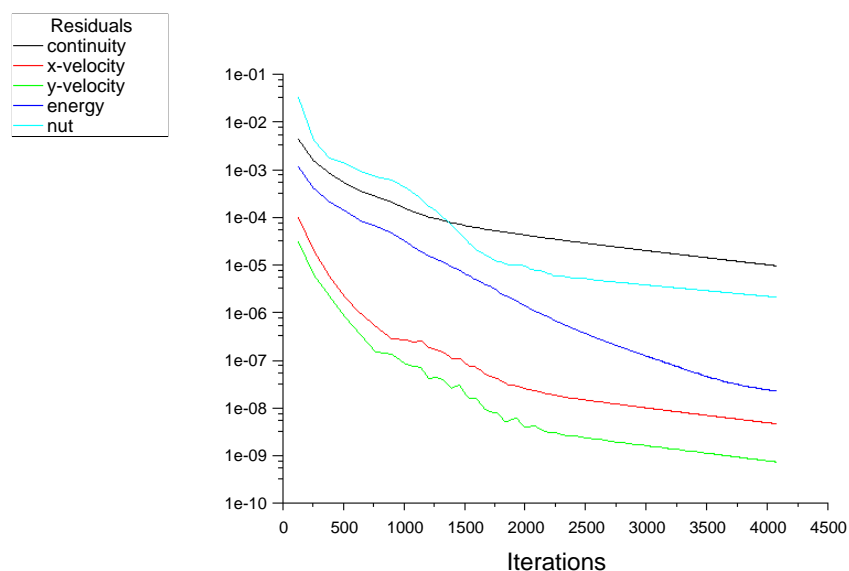


Figure 36: Convergence history of the condiv nozzle.

three axisymmetric and three-dimensional nozzles; they match. The reason could be that the three-dimensional nozzle is not in fact a “real 3d” because a periodic boundary is used in the circumferential direction. A “real 3d” case has not been run because of the mesh generation complexity and computational heaviness (The grid would be over 1.5million of points). What can be hypothesized is that the “real 3d” results would follow the ones seen for the three-dimensional mesh of the inviscid case and therefore that the axisymmetry and three-dimensional sector fail to

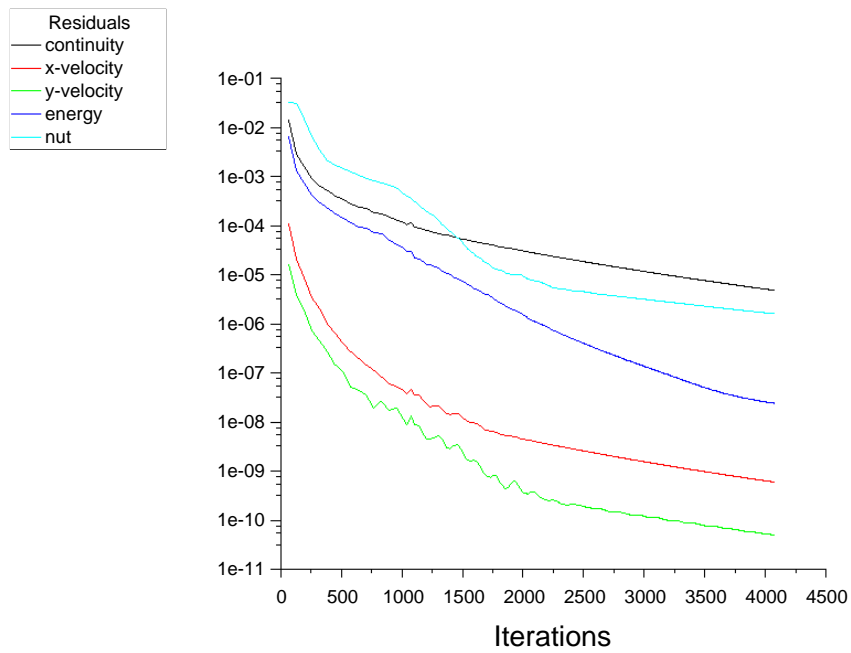


Figure 37: Convergence history of the convlin nozzle.

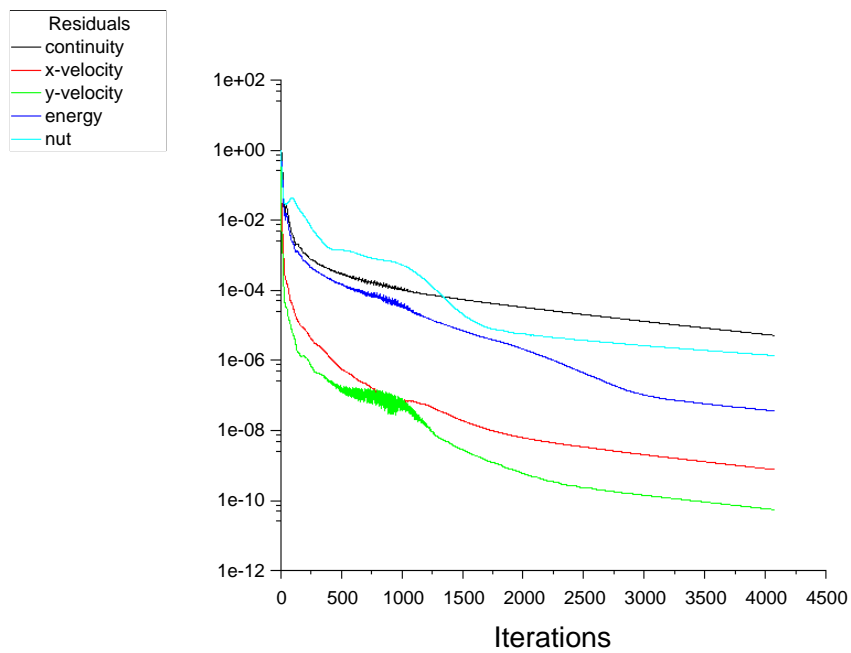


Figure 38: Convergence history of the linear nozzle.

predict the real behavior due to some problem in their boundary conditions along the

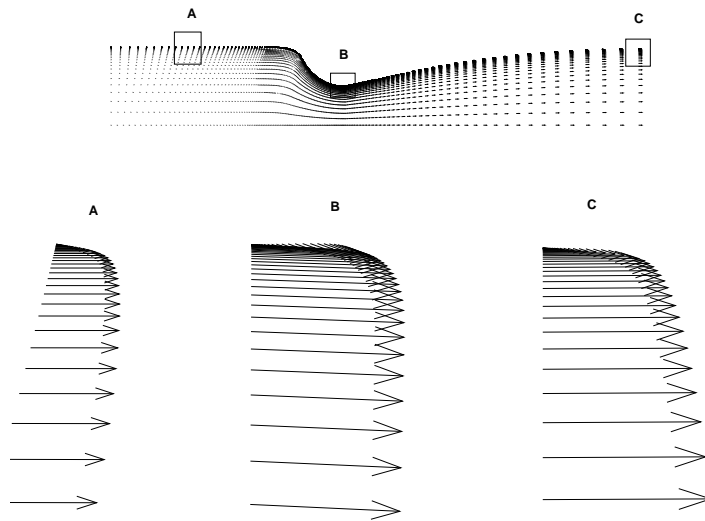


Figure 39: Vectors on the convdiv nozzle.

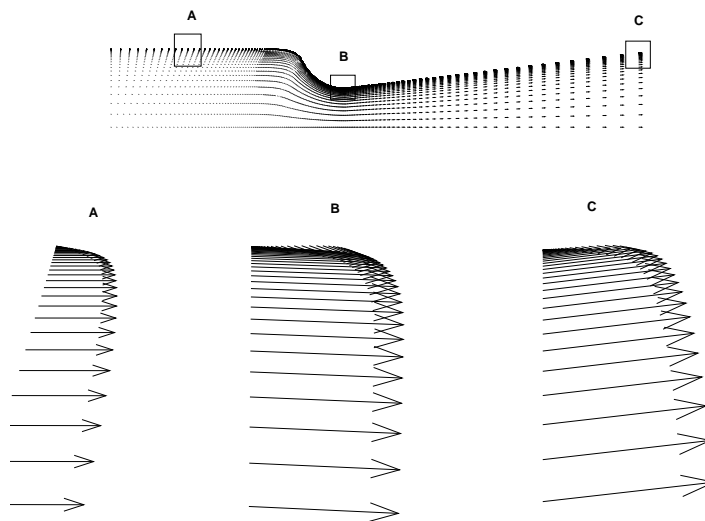


Figure 40: Vectors on the convlin nozzle.

circumferential direction.

The Mach number fields for the axisymmetric grids are drawn in figure 44.

The static temperature and pressure along the axis for the three axisymmetric nozzles are plotted in figures 46 and 47 respectively. The same considerations made

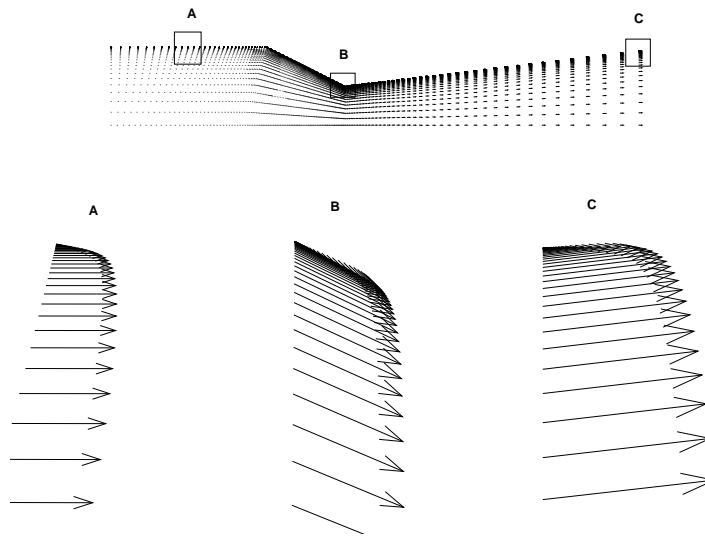


Figure 41: Vectors on the linear nozzle.

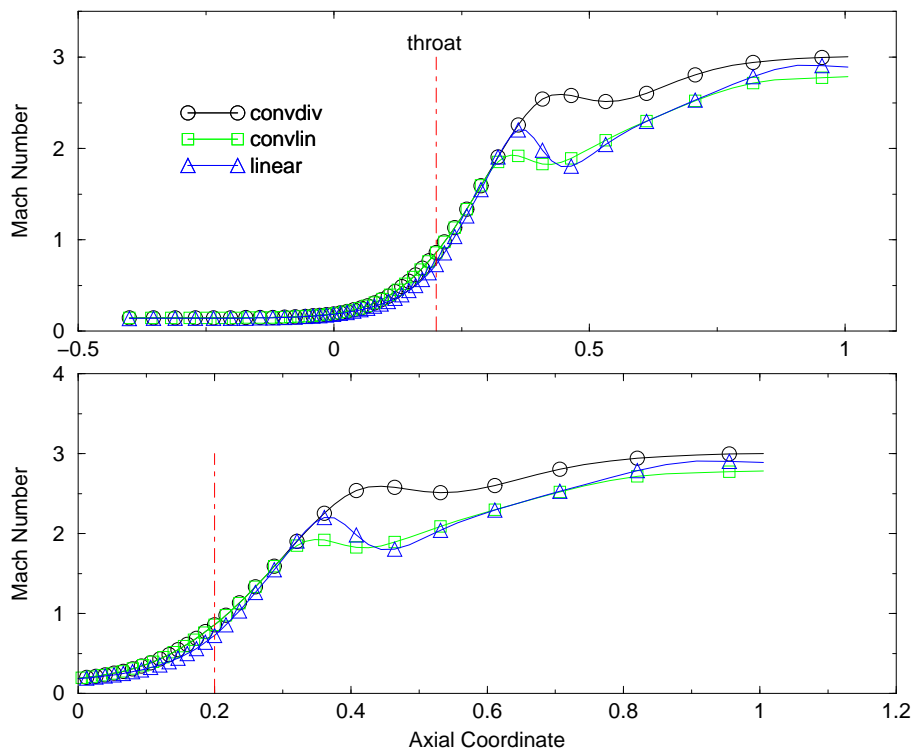


Figure 42: Mach Number along the axis line for the three nozzles.

for the inviscid case may apply for the viscous case.

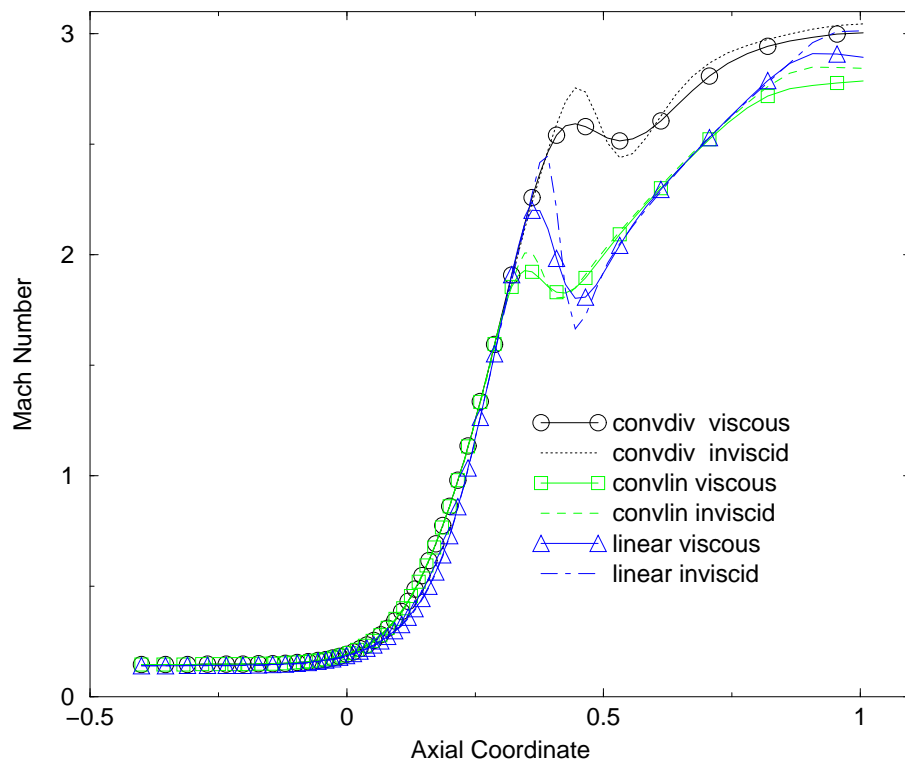


Figure 43: Mach Number comparison between viscous and inviscid computation on the three nozzles.

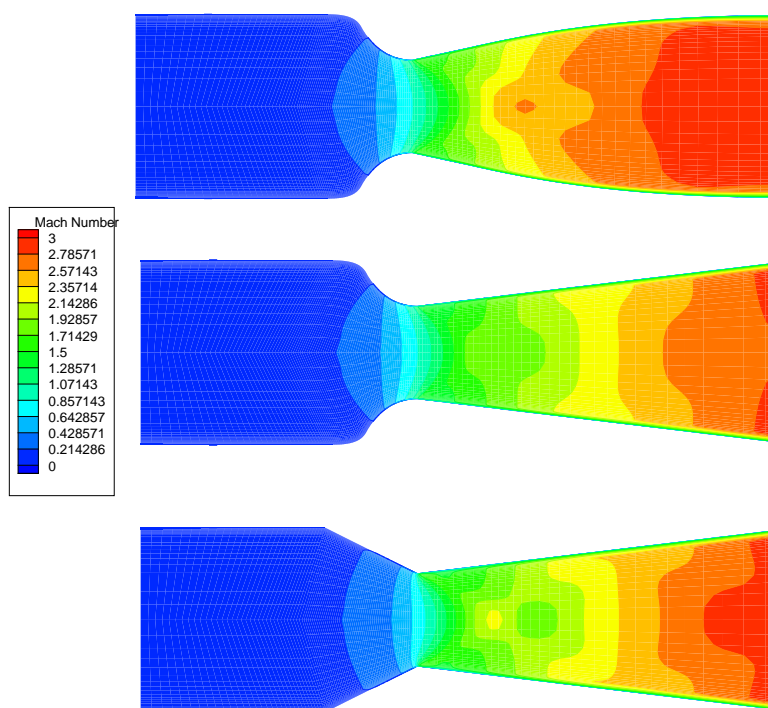


Figure 44: Mach Number fields for, from top to bottom, the condiv, the convlin and the linear nozzle.

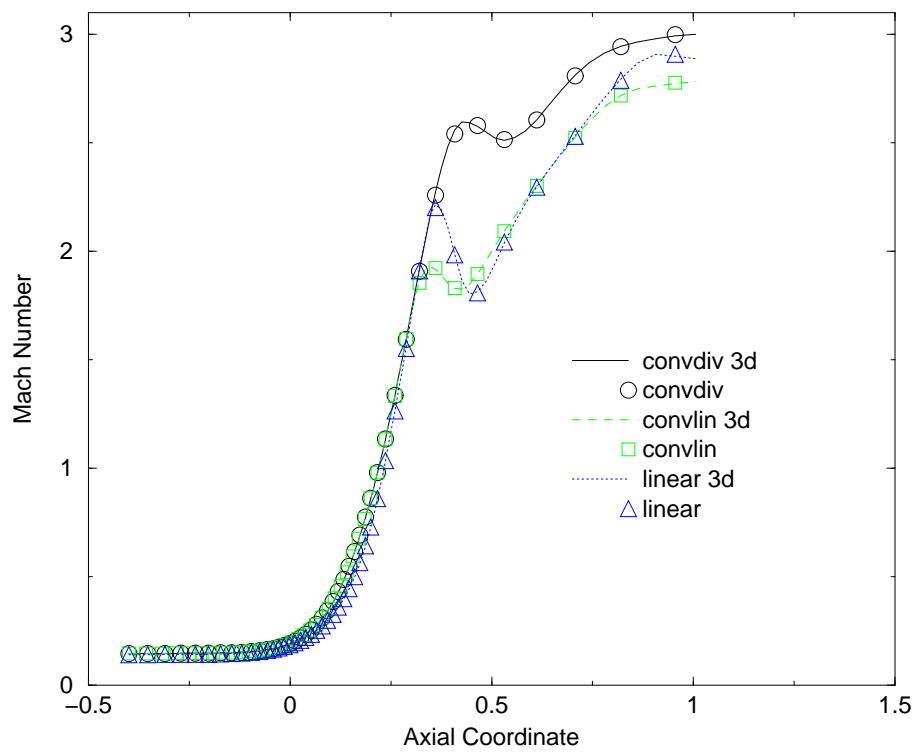


Figure 45: Mach Number comparison between 3d sector and axisymmetric results on the three nozzles.

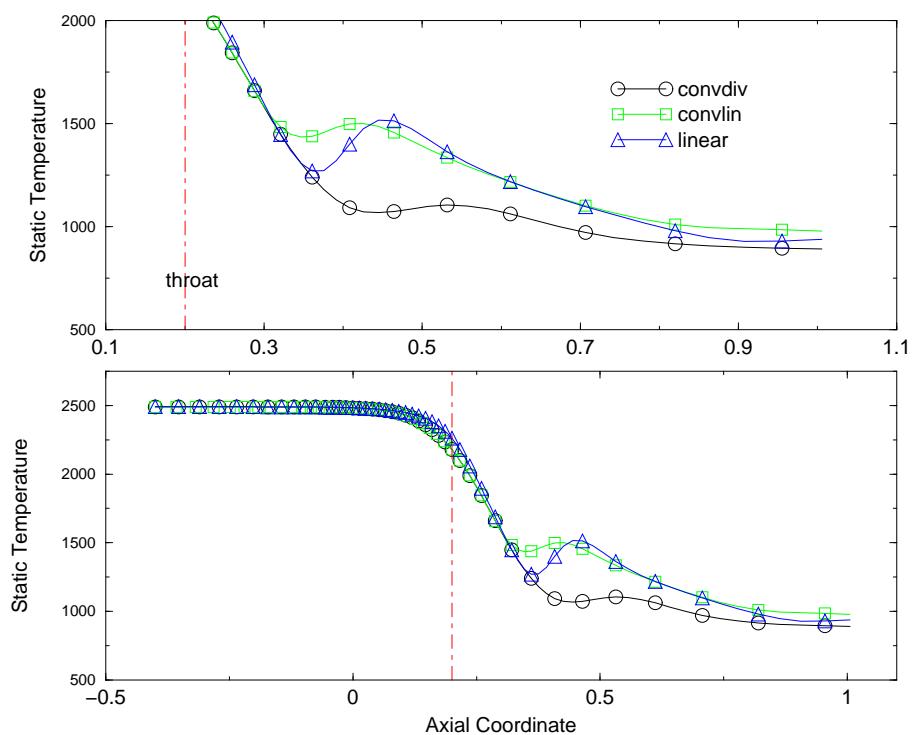


Figure 46: Static Temperature along the axis for the three nozzles.

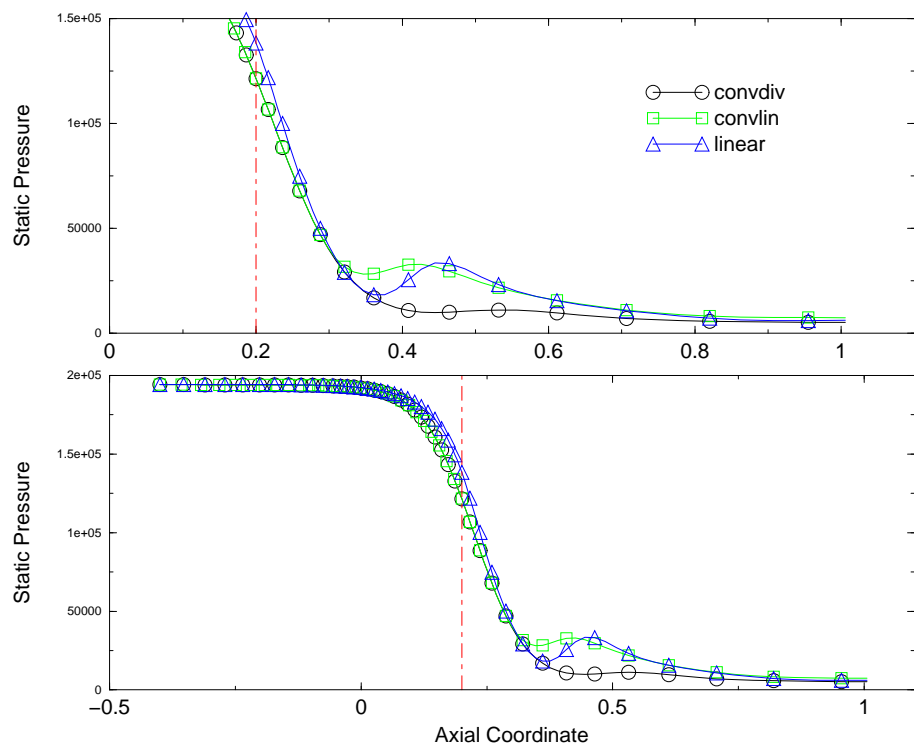


Figure 47: Static Pressure along the axis for the three nozzles.

5 Conclusions

A method to design the convergent and the divergent sections of an inviscid axisymmetric supersonic nozzle has been presented. The results on the test case hereby presented seems to promote both a careful pressure based designed nozzle and a linear one. In the divergent section the designed nozzle has the advantage of getting velocity vectors more aligned along the axial direction while the flow quality seems to be slightly affected.

The final nozzle design must deal with viscosity. In this paper the inviscid design has been tested in a viscous flow. The results seems to follow the same behavior of the inviscid case.

References

- [1] H. W. Liepmann, A. Roshko : Elements of gasdynamics, Published by John Wiley 1957
- [2] J.D.Anderson Jr: Modern compressible flow, Published by McGraw-Hill 1990
- [3] J.J.Korte :Inviscid design of hypersonic wind tunnel nozzles for a real gas , AIAA-2000-0677
- [4] Fluent Incorporated : FLUENT 5 User's Guide, July 1998
- [5] L.Biagioni: Mochpluh User's Manual, May 1997
- [6] F.Scortecci, F.Paganucci, L.Biagioni, S.Borreli, M.Marini: Disegno dell'ugello per una galleria ipersonica ad alta entalpia, 1995
- [7] D.B.Atkinson, M.A.Smith: Design and characterization of pulsed uniform supersonic expansion for chemical applications, American Institute of Physics June 1995
- [8] Devenport: Nozzle applet instruction,
<http://www.engapplets.vt.edu/fluids/CDnozzle/cdinfo.html> March 2001
- [9] R.A. O'Leary, J.E.Beck: Nozzle design ,Rocketdyne's engineering journal of power technology Spring 1992,
<http://engineeringatboeing.com/articles/nozzledesign.jsp>
- [10] M.Mulas: Thermo fluid dynamics of rocket propulsion, Technical Note ASI/WG-09 December 1998
- [11] C.S. Craddock: Computational optimization of scramjets and shock tunnel nozzles, Thesis at the Department of Mechanical Engineering The university of Queensland August 1999